AFM Force Mapping Analysis of an Adsorbed Surfactant Above and Below the CMC

JJ Hamon, Rico F. Tabor,[¶] Alberto Striolo,[‡] and Brian P. Grady[*]

School of Chemical, Biological and Materials Engineering and Institute of Applied Surfactant Research, University of Oklahoma, Norman, Oklahoma 73019. [‡] Department of Chemical Engineering, University College London, London WC1E 7JE, United Kingdom, [¶]Monash University *corresponding author.

Abstract

Force curves collected using an atomic force microscope (AFM) in the presence of adsorbed surfactants are often used to draw conclusions about adsorbed film packing, rigidity and thickness. However, some noteworthy features of such force curve characteristics have yet to be thoroughly investigated and explained. In this work, we collected force curves from tetradecyltrimethylammonium bromide (TTAB) films adsorbed on highly ordered pyrolytic graphite (HOPG), silica, and silica that had been hydrophobized by functionalization with dichlorodimethyl silane. Break-through events in the force curves from several different trials were compared to show that the break-through distance, often reported as the adsorbed film thickness, increased with concentration below the critical micelle concentration (CMC) but was approximately 3.5 nm on all surfaces between 2× and 10× CMC; an unexpected result because of the different surface chemistries for the three surfaces. We employed an AFM probe with a different force constant (k) value as well as a colloidal probe and the break-through distance remained approximately 3.5 nm in all cases. Gradient mapping, a variant of force mapping, was also implemented on the three surfaces and resulted in a new technique for visualizing adsorbed surfactant *in situ*. The resulting maps showed patches of adsorbed surfactant below the CMC and

revealed that with increasing concentration, the size of the patches increased resulting in full coverage near and above the CMC. These results are, to our knowledge, the first time force mapping has been used to spatially track patches of adsorbed surfactant. Finally, layers of surfactants on an AFM tip were investigated by collecting a force map on a single AFM tip using the tip of a separate AFM probe. A break-through event was observed between the tips, indicating a layer of surfactant was present on at least one, if not both tips.

Introduction

Advances in the field of surfactant research have led to apparatuses that can probe several different properties of surfactant layers adsorbed to a variety of surfaces. Techniques include gravimetric analysis such as the quartz crystal microbalance (QCM)[1-4], reflectivity (neutron reflectivity, optical reflectometry, ellipsometry)[3,5,6], surface or interfacial tension (dynamic contact angle, drop shape analysis, bubble pressure tensiometry)[7], electrostatics (zeta potential)[8,9] and force interaction (atomic force microscopy, surface force apparatus). The use of the atomic force microscope (AFM) in surfactant research has made significant contributions to the understanding of adsorbed surfactant morphologies, dimensions, and orientation. Of specific interest to this study are soft contact imaging and force curves that are used to explore the characteristics of surfactant layers.[10-14]

Early seminal papers in AFM studies of adsorbed surfactants concerned surfactants adsorbed on highly-ordered pyrolytic graphite (HOPG) explored by Manne et al.[15,16] These studies were possible due to the production of an electrical double-layer (EDL) at the surface generated by the surfactants and counter ions adsorbed to the surface. This type of imaging, known as "soft contact imaging", is accomplished by increasing the force applied by the AFM tip until it begins to register a response due to the presence of the adsorbed micelle layer. At this point, any lateral variations in the morphology of the aggregates become distinct. These variations are used to determine the morphology of the adsorbed surfactant aggregates before the tip breaks through the layer and images the underlying substrate. However, this technique lacks accurate information regarding the surfactant layer in the z-direction because it does not contact the surface beneath the surfactant during imaging. Therefore, the initial publication of Manne et al. included a force vs. distance curve and a thorough explanation of the details of such curves,

which was necessary to achieve the required mechanical stability over the adsorbed surfactant necessary for sustained imaging.

Others have imaged surfactants and supported lipid bilayers adsorbed on a variety of substrates using soft contact imaging and force curves with a spectrum of pH, ionic strengths, and temperatures.[11,17-22] The force curves initially used to determine the required force for imaging are now also used to study other aspects of the surface and adsorbed species, such as the stability and electrostatic nature of the adsorbed surfactant and lipid layers.[15,19,23-25] Typical properties obtained from force curves are the break-through force, break-through distance, and adhesion force. The break-through force is the force at which the probe will penetrate the micelle layer to the underlying substrate during scanning; it is manifested as an instability point in the force curve. The break-through distance is the distance between this instability and the point of contact with the underlying surface, and is often taken to represent the thickness of the adsorbed film.[11,13,20,22,24,26-31] However, this assumption is questionable since compression is occurring during the measurement and some have assumed that the distance where the force curve deviates from zero is a more accurate representation of the adsorbed film thickness.[19] The number of publications which utilize the break-through distance as well as the much higher degree of accuracy in the automated determination of the instability point was the reason that the break-through distance is investigated here. Lastly, the adhesion force is the force required to pull the AFM tip off the surface during retraction of the probe.

These properties (although primarily the break-through force) were used by Pera, Franz, Butt, Loi, and others to develop and test theories related to the energetic interactions between the approaching AFM tip and an adsorbed lipid DOTAP or DOPS layer.[26,32-34] The events leading to the instability are thought to start at the point the AFM tip begins to interact with the repulsive

portion of the EDL, giving the curve its initial exponential increase with decreasing separation. At a certain distance the tip physically contacts the micelle layer; with increasing force surfactant is displaced from beneath the tip, and the film ruptures. Künneke et al. expanded on these studies and correlated topography, stiffness and the adhesion force, and did so using the enhanced data collection method known as pulsed force mode (PFM), which increased the speed at which force curves could be collected.[21]

The histogram-based analysis implemented by these and other authors has since been used with several different adsorbed layers of lipids and surfactants, including cetyltrimethylammonium bromide (CTAB), tetratrimethylammonium bromide (TTAB), sodium dodecylsulfate (SDS), and biological lipid layers with varying pH, concentrations of added surfactant and tail lengths.[22,24,27,35-37] From this short overview it is clear that many investigations use the break-through and adhesion forces primarily, while the break-through distance values are commented on but are less used in analysis. If these distance values are mentioned or shown in force curves, they are often very similar (normally around 3.5-4 nm), even for different surfactants or concentrations, and there has yet to be a substantial investigation into their comparability and physical origin.[11,22,24,26-29]

As the prevalence of combination instruments implementing AFM continues to grow (e.g. combination AFM/ellipsometer and AFM/quartz crystal microbalance), the use of force curves to verify thickness models could become more and more useful, making the determination and understanding of the break-through distance more necessary. However, there seems to be some discrepancy in the literature as to whether force curves obtained on adsorbed layers includes some compression distance prior to the instability point and whether the AFM tip used during force curve collection is ‘naked’, in the sense that adsorbed layer thicknesses can be

found without considering if there is surfactant adsorbed on the tip. Regardless, there have been seemingly few in-depth studies performed to determine the effects of the tip or probe used to collect the force curves as opposed to the number of studies that make use of break-through events.

In this work, force mapping was used to gather break-through distance, break-through force, and adhesion force values using different surfaces, AFM probes, surfactant concentrations, and surfactant introduction methods. The identity of the break-through distance was then investigated and compared to the trends observed in the break-through force and adhesion force values, and the utility of AFM in collecting and analyzing this and other properties is reviewed. The implementation of the techniques described here requires little more experience than that of the average AFM user and can be done with any AFM with force curve mapping capability.

Experimental Procedures

Surfactant Preparation

Tetradecyltrimethylammonium bromide (TTAB) was obtained from Sigma-Aldrich and recrystallized three times from ethanol before use. The critical micelle concentration (CMC) was found to be 3.52±0.43 mM using pendant drop shape analysis. No minimum was detected in surface tension, which indicates a relatively pure surfactant. This surfactant was used over the more commonly studied CTAB due to a lower Krafft point (0°C for TTAB versus ~23°C for CTAB), which made working around room temperature less likely to induce a phase change.[38]

AFM Probes and Probe Cleaning

Two types of probes were used throughout the investigation: PPP-BSI (NanoAndMore) and MSCT "f" probe (Bruker). The PPP-BSI probe had a nominal force constant of 0.1 N/m, a

resonant frequency of 28 kHz and tip radius of less than 10 nm and the MSCT probe “f” had a nominal force constant of 0.6 N/m, resonant frequency of 125 kHz, and tip radius of 10 nm. Prior to use, the probes were cleaned in a UV Ozone chamber for 30 minutes.

Colloidal Probe Preparation

The colloidal probe, which was an AFM probe with a spherical glass bead on the end, was prepared by first taking a clean microscope slide and applying a small drop of UV curing glue and using a disposable needle to create glue streaks that were thinner than the initial drop. Around 25 mm away on the same side of the same microscope slide, a small quantity of glass beads (Polysciences, Inc.) were added by quickly inverting and righting the closed bottle containing the beads, removing the cap and tapping it on the glass slide. This procedure provided an array of separated glass beads from which to choose. A PPP-BSI AFM probe was loaded onto the JPK Nanowizard III AFM head and the laser was aligned on the back side. The head was moved towards the surface of the microscope slide using coarse steps until a streak of the UV curing glue was in roughly the same focus as the cantilever of the probe. Using the AFM as a micromanipulator, the AFM tip was moved over the glue streak (using the optical microscope) and then lowered in small increments (5 μm or less) until the deflection moved away from center. If contact with the glue was made, then retracting the probe from the surface would not occur until a few retraction steps were taken because the glue caused the probe to deflect adhesively.

Once the glue was applied to the cantilever/AFM tip, the tip was moved to a glass bead, chosen based on visual inspection of cleanliness and separation from other beads. The cantilever was lowered using small steps until the deflection deviated from zero and in some instances one additional approach step was taken to ensure good contact. A blue handheld laser with a

wavelength of 405±10 nm and a max output lower than 5 mW was then directed towards the AFM probe covered in UV curing glue which was now in contact with the chosen glass bead. The light for the optical microscope used on the AFM was turned off and the blue laser was turned on and positioned so that the reflection of the blue laser could be clearly seen on the viewing screen attached to the optical microscope indicating that the laser was in the right spot to cure the glue. The laser was held here for 1 min and then the optical microscope light was turned back on and the AFM probe retracted 50 μm. If the glass bead went out of focus with the AFM probe then it was successfully attached, otherwise glue was reapplied to the AFM probe and a new bead was found. In most instances, between 1 and 3 attempts were necessary; this lack of consistency likely resulted from the limited contact area of the cantilever tip, which may inhibit effective sticking of the bead. Use of tip-less cantilevers would likely alleviate this issue.

Surface Preparation

Force maps were obtained on highly oriented pyrolytic graphite (HOPG), UV ozone treated silica, and silica reacted with dichlorodimethyl silane (DCDMS). HOPG surfaces were obtained by cleaving the upper layer of a ZYH-grade planchet from Momentive Performance (Strongsville, OH) using double-sided tape. No further cleaning treatment was performed to this surface.

The silica used was cleaved into 1cm x 1 cm surfaces from a 4-inch diameter ellipsometry standard (J.A. Woolam) with a 60 nm thermally grown oxide layer using a diamond tipped scribe. The cleaved surfaces were then cleaned using a methanol soak with sonication to remove any particles present on the surface from the cleaving procedure. DI water was used to rinse the samples, which were then dried in a nitrogen stream. Next, the silica surfaces were placed in a Harrick Plasma Cleaner (PDC-32G) and cleaned using the ‘medium’ setting (10.5 W

applied to RF coil) under vacuum for 10 minutes. The surfaces were then transferred to an 80ºC RCA-1 cleaning solution (1:1:5 solution of NH_4OH:H_2O_2: Milli-Q H_2O) for 25 minutes in a Teflon® sample holder. Next, the surfaces, removed from the solution, were rinsed individually with Milli-Q H_2O and dried under a nitrogen stream. Then they were immediately moved to the plasma cleaner for 5 minutes on the 'low' setting (6.8 W applied to RF coil) and finally removed to fluoroware for storage until use. Before a silica surface was used from storage it was exposed to UV ozone for 45 minutes and then placed at the bottom of the dish before adding surfactant solution.

To obtain a silanated silica surface, a silica surface cleaned in the manner described above was exposed to dichlorodimethyl silane vapor post UV ozone treatment by holding the silica surface inverted in the mouth of the silane bottle for 30 seconds. No further cleaning treatment was performed on the silanated surface.

The contact angles of water on the three surfaces post treatment were measured using the sessile drop method and are given in Table 1. The results agree well with literature values using the same surfaces.[39,40] The results showed that the silanated silica had the most hydrophobic character of the three surfaces used followed by HOPG. The UV ozone cleaned silica sample was completely wetted by water and was therefore the most hydrophilic.

Table 1	
Silanated Silica	96.1
HOPG	62.0
UV Ozone Silica	~0 (completely wetted)

Table 1. Contact angle of 18 MΩ water on silanated silica, HOPG and UV Ozone cleaned silica.

Surfactant Soft Contact Imaging

Soft contact imaging on HOPG and silica was performed using a JPK Nanowizard III (Berlin, Germany) AFM and PPP-BSI probes. To image surfactant assemblies on these surfaces the probe was approached and then image collection begun. The setpoint was decreased during

scanning until the tip came fully away from the surface, overcoming adhesion forces, and then the setpoint was increased until surfactant was observed. An easy verification that surfactant is being imaged and is not an artifact is by changing the scan angle and size. If changing these parameters produces no apparent variation in the image, then the image features are most likely either artifacts or caused by feedback due to inaccurate tuning parameters.

Concentration and Probe Switching Methods

Batch Method

The simple setup of the batch method (a dish and surfactant solution) and the potential for combining data from several trials makes the batch method an attractive means of collecting force curve data with surfactants. The surface was placed (double-sided tape was only used in the case of HOPG) at the bottom of a clean glass dish large enough to accommodate the AFM head and then the surfactant solution at the proper concentration of surfactant was added. The probe then approached the surface and force maps were collected. Then the probe was retracted and the solution and submersed surface were removed before a separate dish with a separate surface in a separate aliquot of the surfactant solution was put in its place. The probe was also removed from the AFM head, UV Ozone cleaned and then put back in the AFM head (or a different probe also UV Ozone cleaned was placed in the AFM head) before approaching.

Perfusion Method

The perfusion method, although having a more complicated setup than the batch method, ensures the collection of data from the same location between trials and removes the effects of tip cleaning and concentration switching. The perfusion method was carried out using the same glass dishes as used in the batch method, but syringes connected to Teflon® tubing were used to inject the solutions into the cell on one side of the dish and withdraw it from the other, removing the need to move the AFM tip laterally allowing for force maps and imaging to be performed in the same exact spot at different surfactant concentrations. First, water was injected into the cell

and force maps were collected before retracting the AFM probe by 5 μm. Then the syringes placed in the dish were used to remove the solution in the dish at the same rate that the new solution, in this case 0.2×CMC TTAB, was injected. When twice the volume of the dish had been perfused, the system was left unperturbed for 10 minutes to allow for equilibration and then the AFM tip was approached and mapping or imaging was performed. Each map took approximately 20 minutes to collect and in some cases a map was collected immediately following another map. Comparing subsequently collected maps allowed for following the time evolution of adsorption or location of specific patches of surfactant. This procedure was repeated for the whole concentration series, which began with water and was increased by 0.2×CMC until 0.8×CMC and then the concentration was further increased to 2×CMC and then 5×CMC and finally 10×CMC.

Force Mapping on Various Surfaces

The force mapping feature of the Nanowizard software was used to obtain a 32×32 grid of force curves in desired areas with varying map sizes on HOPG, silica, and silanated silica using both the PPP-BSI probes and the "f" cantilever on a MSCT probe. Before use, each probe was calibrated to determine the deflection sensitivity and the force constant by obtaining a force curve on a clean microscope slide and fitting the gradient (slope) of the line where the probe was in contact and then by using the thermal method, respectively.

The probes were used only if the measured force constant fell within the specification parameters (~ 5 percent of the probes did not meet this criterion). The deflection sensitivity was measured again in solution on the substrate prior to any other measurements. Note that the cantilever shape for the PPP-BSI probe is rectangular while the MSCT cantilever is triangular; although this could cause a difference in the lateral bending of the cantilever, we are only using

the vertical deflection for analysis and therefore the difference in shape should not be an issue if the force constants are known.

The curves in Figure 1 show the difference between a force curve obtained in water (Figure 1a) and one obtained in an aqueous medium containing surfactants (Figure 1b). The former shows only a snap to contact at ~5 nm caused by attractive surface forces while the latter shows a repulsive force beginning at approximately 15 nm (generated by the electrical double layer near the surfactant assembly) and ending with an instability at ~4 nm. Following the instability, the probe is in contact with the substrate underneath the surfactant layer. The force at which the instability occurs is taken to be the break-through force while the distance between the instability point and the substrate is taken to be the break-through distance. Each force curve within a force map was obtained with a tip velocity of 700 nm/s and over a range of 500 nm. The relative force setpoint (the force at which extension of the probe was stopped and retraction begun) was varied based on the force required to obtain a sufficient number of points post break-through, usually between 3 nN and 8 nN.

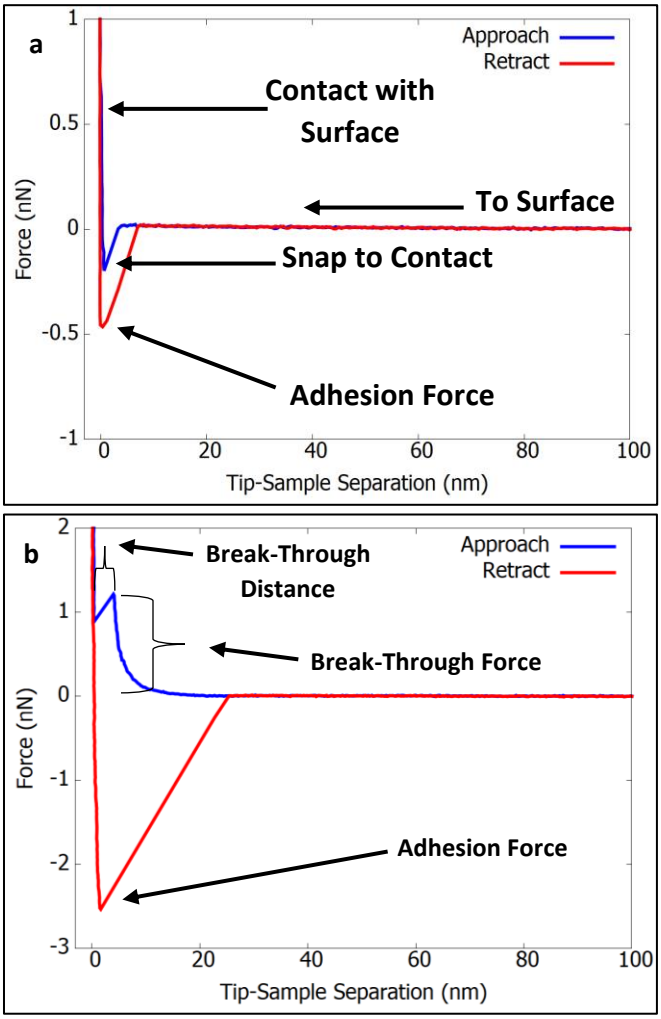

Figure 1. Diagrams identifying key parts of AFM force curves. Top: water. Bottom: surfactant solution.

Once the probe reached this setpoint, it was retracted from the surface. Due to adhesive forces between the surface and the probe there was a distance during which the probe remained on the surface past the point of zero deflection. A snap-off the surface occurred once the force necessary to overcome adhesion was applied and resulted in a minimum in the force curve, which was taken as the adhesion force. In a force curve, a negative force is attractive, however, we will discuss both the break-through force and adhesion force as positive values given the conventions typically used for both forces.

Automated Analysis Post Collection (Python and Gaussian Fitting)

Post collection, the JPK data processing software was used to convert the gathered deflection and distance data into force and tip–sample separation before exporting each curve as a separate text file. The force curves were then analyzed using scripts developed in Python, which first separated the data into approach (extend) and retract curves and then identified the break-through points to obtain break-through distance, break-through force, and adhesion force. The data obtained from each force map was used to create histograms, which summarize the break-through distance, break-through force and adhesion force acquired from the force maps. Our analysis operates under the assumptions outlined by Butt and Franz, specifically that there is a probability distribution which describes the point at which the tip will break through the surfactant layer, and therefore a range of values are possible for any trial.[26] The histograms were then fit to a normal distribution using equation 1, where A is the normal distribution peak maximum and μ and σ are the mean and standard deviation respectively.

$$y = A \cdot \exp\left(-\frac{(x-\mu)^2}{2\cdot\sigma^2}\right) \qquad \text{eq.1}$$

The fitted values were then compared using a variety of concentrations, surfactants and surfaces. In the event of multiple peaks, equation 2, which uses the same variable designations

as equation 1, was used to fit the histogram data,

$$y = A_1 \cdot \exp\left(-\frac{(x-\mu_1)^2}{2\cdot{\sigma_1}^2}\right) + A_2 \cdot \exp\left(-\frac{(x-\mu_2)^2}{2\cdot{\sigma_2}^2}\right) \qquad \text{eq. 2}$$

Results and Discussion

AFM Force Mapping of an AFM Tip

Unless explicitly stated, throughout this paper the terms monolayer and bilayer refer to the number of layers forming the structures on the surface (e.g. monolayer refers to flat monolayers as well as hemi-cylinders and hemi-spheres, while bilayer refers to a flat bilayers as well as full cylinders and spheres). We have no reason to believe that our methods can distinguish the various types of single-layer type structures from one another, nor the various types of multilayer-type structures from one another.

Many previous publications interpret the break-through distance as the thickness of the adsorbed surfactant layer directly, which assumes there is no surfactant adsorbed to the probe. However, Ducker et al. investigated the surfactant adsorbed to the tip by collecting force curves, however without collecting a force map, on a silicon nitride surface using a silicon nitride probe with the zwitterionic surfactant dodecyl dimethyl ammoniopropanesulfonate.[41] They assumed that using the same material would yield similar structures on both the tip and the surface and determined that the thickness measured using force curves was based on the applied load. The latter conclusion is a result of designating thickness as any point between the point of initial increase in force and the instability point and not the break-through distance. In our work, this method of using a probe and surface of the same material is taken a step further by mapping an AFM tip using another AFM tip in 10×CMC TTAB solution, which provides not only the same material, but also the same surface geometry. Only single force curves could be obtained at the tip-

tip interaction as compared to 1024 curves we could obtain for flat surfaces; therefore, similarly robust statistical data-sets were not possible. However, our data demonstrate the concept of force mapping on an AFM tip, and they permit to draw conclusions based on the presence and appearance of break-through phenomena.

The mapping probe was positioned over the to-be-mapped probe using a top-down optical microscope. The to-be-mapped probe was prevented from deflecting away from the mapping probe by positioning it over the chip portion of a separate AFM probe (see Figure 2a), which, by design, was at the same height as the underside of the AFM cantilever. Prior to mapping the tip, a 32×32 force map was collected on the cantilever of the probe being mapped. This was obtained as a benchmark comparison to a flat surface of the same material at the same time and with the same probe being used to map the tip surface. The break-through distance, break-through force, and adhesion force were found to be 3.39 nm ± 0.61 nm, 0.33 nN ± 0.04 nN and 0.05 nN ± 0.007 nN on the cantilever, respectively.

Next, the tip itself was mapped using a 16×16 force mapping grid. The smaller grid size was used on the tip because a 32×32 grid experienced significant drift during the experiment.

Even with the smaller map there was still a fair amount of drift, likely due to mechanical coupling within the complex arrangement of cantilevers and chips, but it was less of an issue because of the increased speed of collection with the smaller grid. Of the 10 maps collected, 3 were successful in collecting a force curve at the apex of the two tips.

The maps and a representative force curve are shown in Figure 2. The curves collected at the maximum height of the maps did display break-through forces above zero, indicating the presence of a repulsive force near the surface.

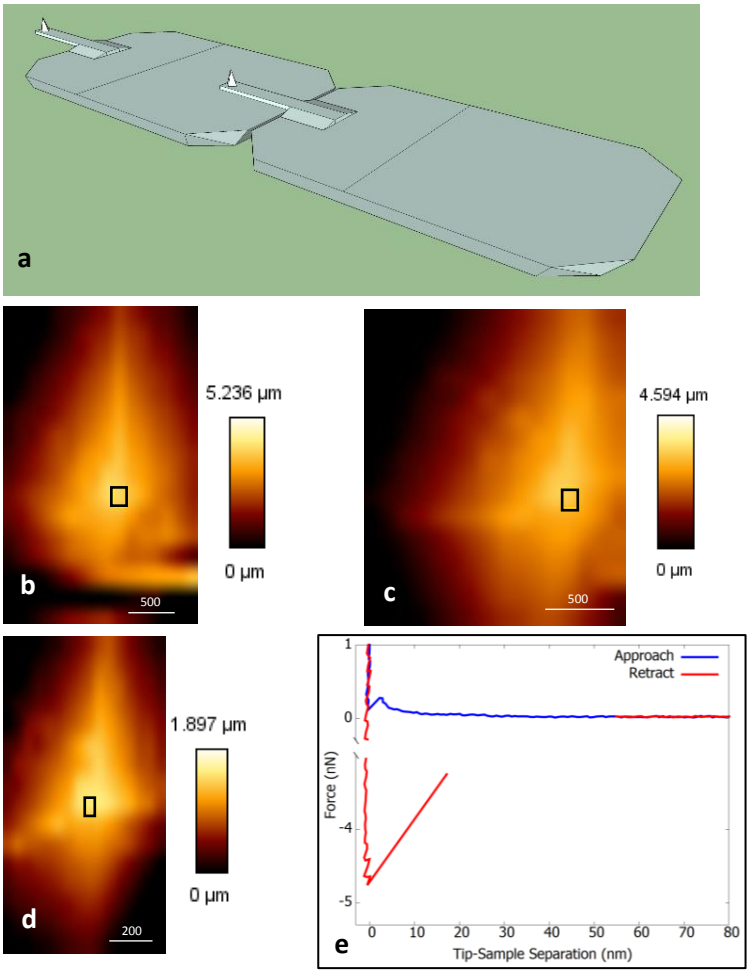

Figure 2. (a)-Scheme showing the AFM tip to be mapped positioned over the chip of another AFM probe to prevent deflection during mapping.

(b), (c), (d)-the three (separate) successful force maps of a PPP-BSI probe in a 10×CMC TTAB solution. the black boxes in the images are the point of maximum height measured value, taken to be the interaction between the two tips.

(e)-Example force curve (with a split y-axis) from between the two AFM tips at the maximum height.

The break-through distances, break-through forces, and adhesion forces for the three maps were found to be (3.3 nm, 0.28 nN, and 4.76 nN), (4.29 nm, 0.18 nN, and 2.23 nN), and (5.05 nm, 0.65 nN, and 0.33 nN), respectively.

Although there is substantial variation in these measurements, our results indicate that there is adsorbed surfactant with some thickness present. The symmetry of the system strongly supports the possibility of an adsorbed layer on both tips. This layer is assumed to be a monolayer, since it has been previously stated that AFM tips should be incapable of supporting the formation of a bilayer without chemical modification.[42] To investigate surfactant adsorbed to a different type of probe, a colloidal probe was used on a flat HOPG surface.

Colloidal Probe Trials

A 58-µm colloidal sphere attached to PPP-BSI AFM tip was used and the results of a 32×32 force map obtained in 10×CMC TTAB using this colloidal probe on the TTAB layer on HOPG are shown in Figure 3. The force curve shown, Figure 3a, had a low gradient region at 3 nN, which was taken to be the break-through event. The break-

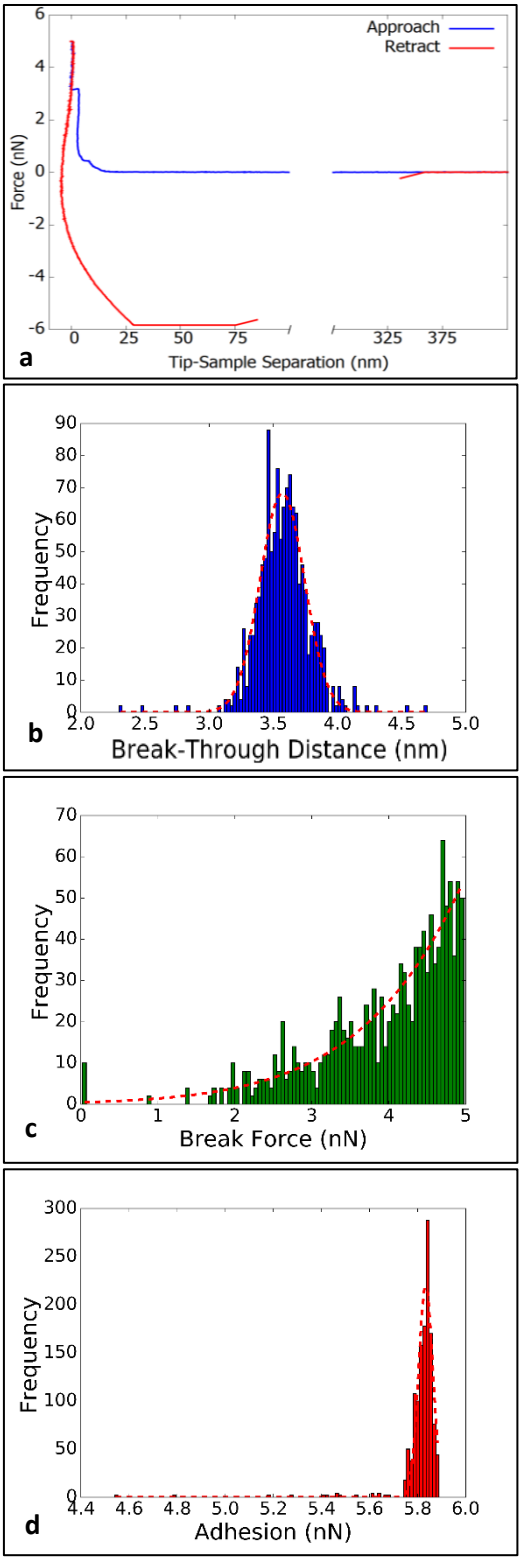

Figure 3. Example force curve (with split x-axis) and histograms of break-through distance, break-through force and adhesion for a colloidal probe on HOPG with 10×CMC TTAB

through force was found to be ~3 nN in this curve and the retraction curve had noticeable bowing leading up to a flat region at 6 nN. This flat region was caused by the measured value exceeding the limit of the measurable deflection (12 V, which corresponds to 6 nN after accounting for deflection sensitivity). The break-through distance obtained from the histogram in Figure 3b was 3.57 nm ± 0.17 nm, which is in the same range as values found in literature using various surface geometries. [11,37,43] As with the force curve, the histograms in Figure 3c and Figure 3d demonstrate how the measurable deflection limit affected the break-through force. Below the instrument limit of 5 nN the break-through force histogram shows what appears to be half of a normal Gaussian curve.

The low gradient at the break-through event resembles the curves found by Donaldson et al. when using a surface force apparatus (SFA) to study azo-TAB on mica.[44] In their work, there was a distinct difference in the appearance of the force curve and the break-through force for a light-switchable surfactant monolayer or bilayer. In the case of the bilayer, the break-through force was greater, and the force curves had a much lower gradient at the break-through event. Compared to the force curves found here, there is a resemblance between our colloidal probe curve profile and the azo-TAB bilayer, which would suggest hemifusion is occurring here, as was concluded in theirs and other work.[45]

Hemifusion, represented in the scheme given in Figure 4, describes what happens when two hydrophilic surfaces, each supporting a bilayer, come into close contact. The repulsive forces generated by the bulk-facing headgroups lead to disruption of the opposing bilayers, resulting in the compression and rearrangement of the two separate aggregate layers to form a

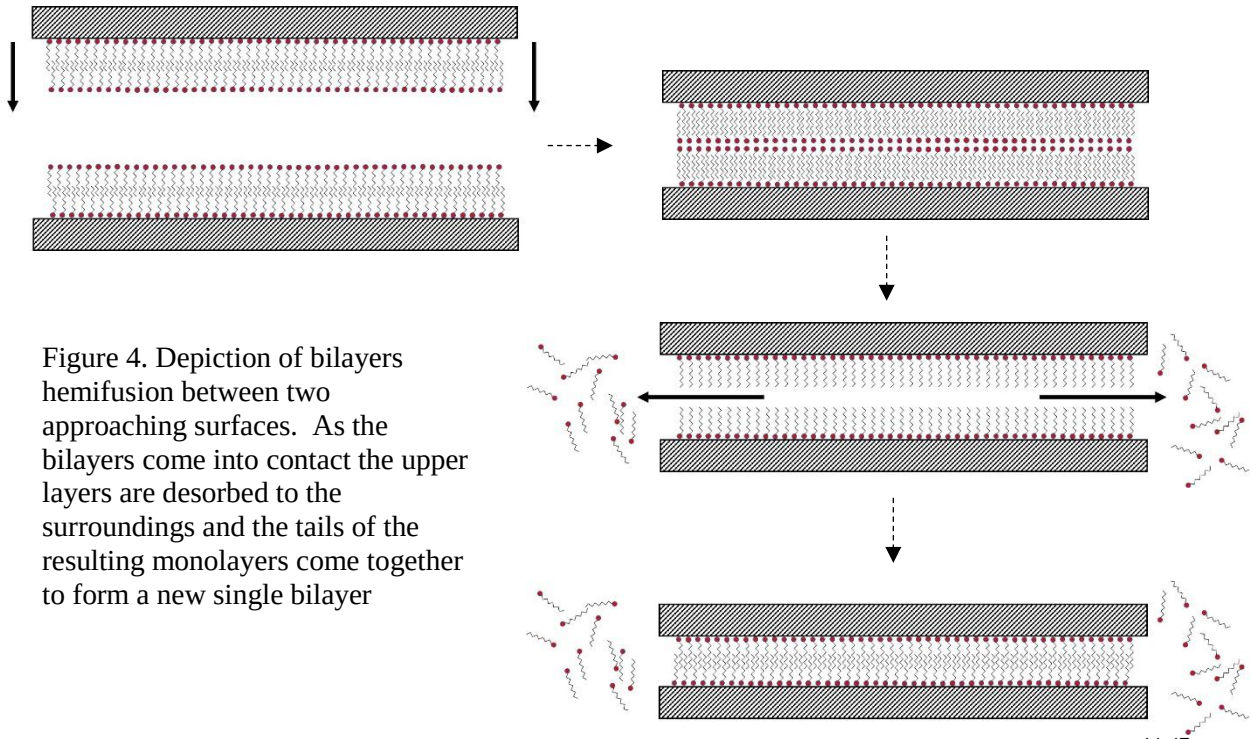

Figure 4. Depiction of bilayers hemifusion between two approaching surfaces. As the bilayers come into contact the upper layers are desorbed to the surroundings and the tails of the resulting monolayers come together to form a new single bilayer

single layer between the two surfaces, with the simultaneous ejection of some surfactant.[44-47] Hemifusion also implies that adsorbed surfactant morphologies may change through interaction with another surface (two bilayers initially and one bilayer after interaction). Visual inspection of the force curves presented in the work of Donaldson et al. suggests a break-through distance (jump-in), which is approximately equal to the hemifusion distance, suggesting the possibility that the break-through distance represents the hemifusion distance rather than the surfactant layer thickness. However, previous work differs substantially from the work described in this section. Since HOPG has been shown to support the formation of a monolayer surfactant structure; i.e. instead of two bilayers with two mica SFA surfaces the expected situation with HOPG and our colloidal probe is a monolayer and a bilayer. However, the measured break-through distance is characteristic of bilayer thickness, not monolayer plus bilayer. To further investigate the identity of the break-through distance, force maps were collected on HOPG using regular AFM probes.

Flat Surfaces Sampled with Regular AFM Probe

HOPG Above the CMC

The data shown in Figure 5 represent the break-through event parameters for 10×CMC of TTAB on HOPG from a force map with side lengths of 500×500 nm. The mean and standard deviation from fitting the break-through distance, break-through force and adhesion force histograms were found to be 3.25±0.31 nm, 1.18±0.18 nN and 2.49±0.2 nN, respectively. Imaging at this concentration showed parallel rows of surfactant arranged in different orientations caused by grain boundaries on the HOPG surface, which agrees with imaging found in previous investigations.[15] The parallel alignment and even spacing of the rows are due to the surfactant adsorbing conformally with the symmetry axes of the graphite substrate.[12,48] Fast Fourier

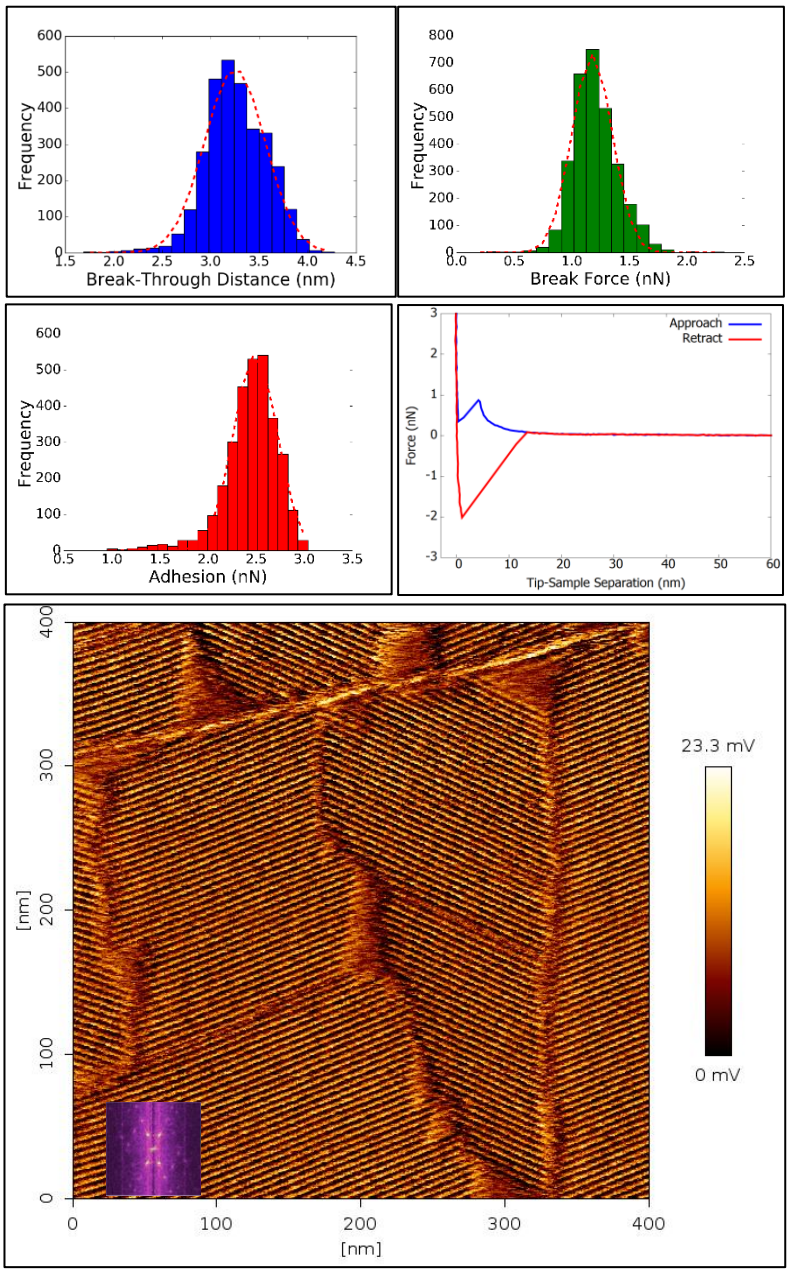

Figure 5. Histograms with Gaussian fitting results (red dotted line) and soft contact image of 10×CMC TTAB on HOPG with PPP-BSI probe

Transform (FFT) analysis (overlay in the lower left of the soft contact image in Figure 5) was used to determine the period (rationalized as the sum of the width of a micellar aggregate and distance between aggregates), which was 4.7 nm, matching values found in the literature.[16]

Comparison of several surfactant break-through distance values on HOPG shows a similar range of values as observed in our work, suggesting that a future force mapping/histogram study involving surfactants of various chain length and headgroup charge would be beneficial in verifying the nature of the break-through distance.[14,15,31,41,49]

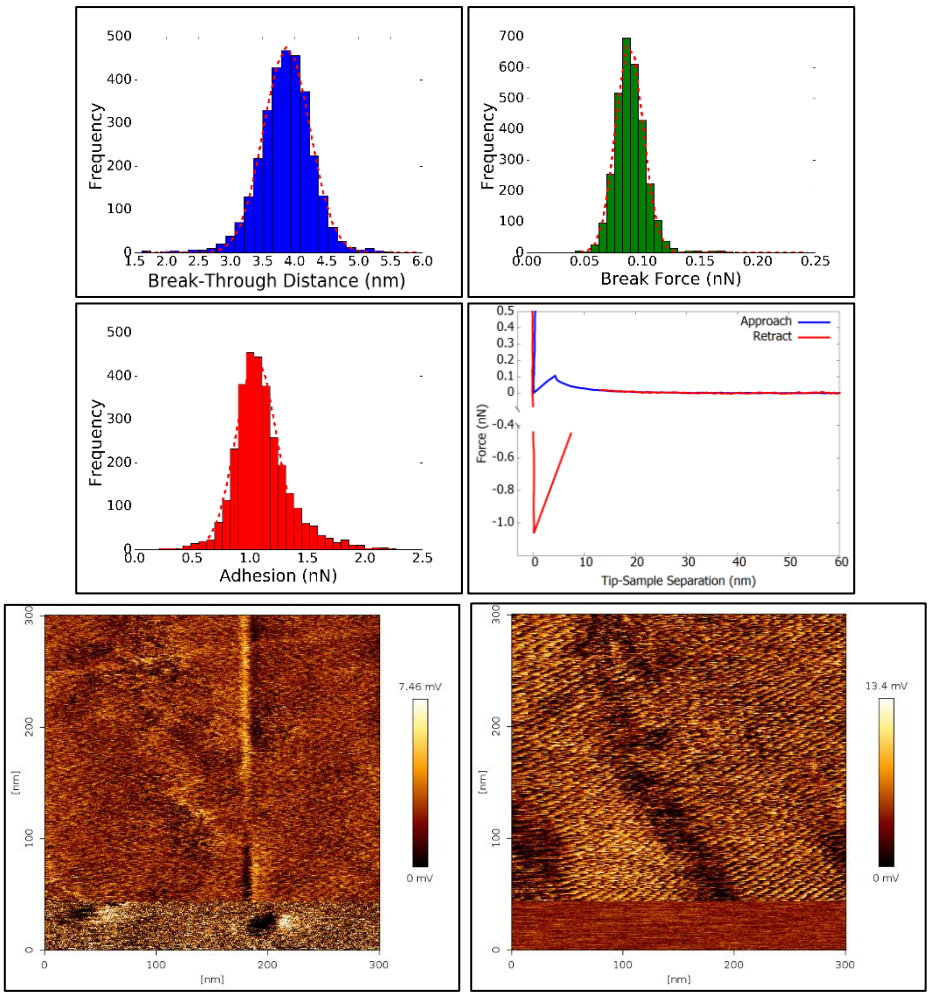

Figure 6. Histograms of break-through distance, break-through force and adhesion force of 0.5×CMC TTAB on HOPG along with the Gaussian fit results (red dotted line) and an example force curve (with split y-axis). Below are the error (left) and lateral deflection (right) images at the same concentration. In these images the scan direction is from bottom to top.

For the purposes of this paper, it is noted that the HOPG break-through values obtained using the regular AFM probe here are like those found on HOPG using a colloidal probe discussed above. It is well accepted that ionic surfactants form monolayers or hemi-spheres/hemi-cylinders on hydrophobic

surfaces (e.g. HOPG) and bilayer or full sphere/cylinder aggregates on form on hydrophilic surfaces.[5,13,50,51] Therefore, this agreement is surprising; for the case of a colloidal probe and HOPG a bilayer and a monolayer are expected while in the case of an AFM tip and HOPG a monolayer and a monolayer are expected. Therefore, we expected a greater break-through distance for the colloidal probe vs. the normal AFM tip. This curious discrepancy will be elaborated upon in the "further discussion" section.

HOPG below the CMC

Adsorption of 0.5×CMC TTAB on HOPG was investigated using a 500×500 nm side length force map and soft contact imaging, and the results are given in Figure 6. The mean break-through distance, break-through force, and adhesion force were found to be 3.88±0.37 nm, 0.09±0.012 nN, and 1.06±0.17 nN, respectively. The break-through distance obtained at 0.5×CMC is about 0.5 nm higher than that obtained at 10×CMC TTAB, while the break-through force is 10% that obtained at 10×CMC. The large difference in break-through force was expected, given that SFA experiments showed a drop in break-through force below the CMC to 15% of the value measured above the CMC.[37] Given the patchy nature of adsorption that will be proven later in this paper, the low break-through force is likely a result of surfactant being more easily moved by an approaching AFM tip.

With soft contact imaging, scanning 'above' the surfactant layer without breaking through to the underlying substrate was difficult below the CMC. The typical indication of break-through during scanning was the disappearance of surfactant from the image (either in height or error signals) mid-scan, or a sudden change in the lateral deflection signal (i.e., increased friction once the probe contacts the surface). Also, there was very little resolution of surfactant in the height or error images until post break-through, after which the parallel lines of

surfactant are observable, albeit with rougher edges between the rows of surfactant when compared to images obtained above the CMC.

The ability to image surfactant aggregates below the CMC indicated that the surface concentration where cooperative interactions are responsible for adsorption of TTAB was less than 0.5×CMC, which is not surprising given that SDS has been imaged at 1/3 of its CMC.[49] As the surfactant assemblies on the surface are patchy below the CMC, the approach of an AFM tip could cause dynamic surface reconfiguration, a process which is expected to be much faster than scanning timescales (individual surfactant adsorption-desorption times tend to be on the order of milliseconds). Therefore, a probe at the hard surface could be scanning within the micelle layer, which could yield a variation in the friction sampled by the probe, accounting for the similar imaging in the friction signal post break-through (bottom right image in Figure 6).

HOPG Concentration Gradient

Next, a concentration gradient was performed using the batch method of data acquisition. The data in Figure 7 show break-through distance, break-through force, and adhesion force for TTAB on HOPG for concentrations between 0.5×CMC and 10×CMC using two different PPP-BSI probes, nominally with the same characteristics. The break-through distance did not change appreciably over the concentration range from 0.7×CMC to 10×CMC,

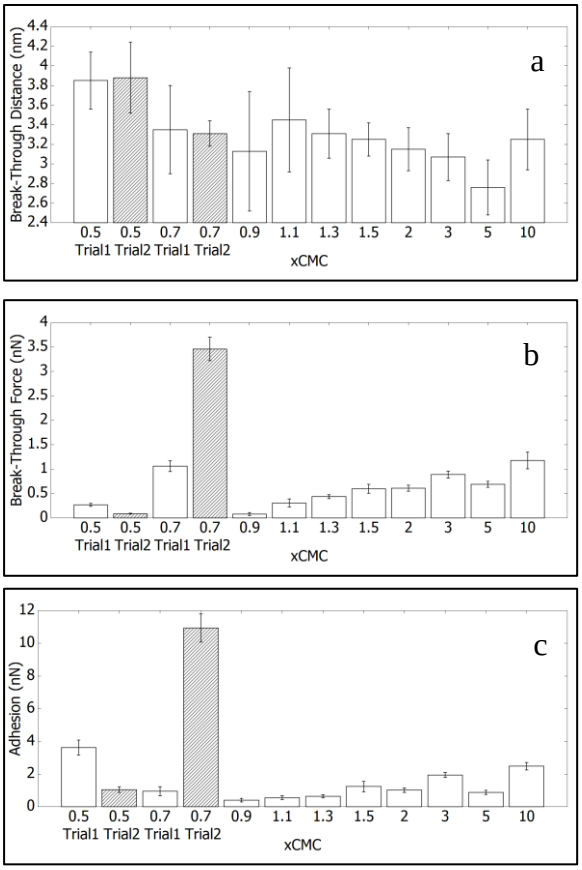

Figure 7. Break-through distance (a), break-through force (b) and adhesion (c) results for various concentrations of TTAB on HOPG. Different colors represent different probes.

remaining between 2.8 nm and 3.4 nm. Ignoring the data at 0.7×CMC, the break-through force does seem to increase with concentration through the CMC. This result differs from a previous SFA investigation for lipid bilayers, in which the break-through forces below the CMC varied and achieved a plateau above the CMC.[37] However, the behavior of the break-through force with concentration was also measured with different results in perfusion experiments, which will be detailed later. Comparing different concentrations in perfusion experiments is expected to yield better results vs. comparing different concentrations in batch experiments as will be discussed more completely below.

The clear difference in break-through force and adhesion force values for trials 1 and 2 of the 0.5×CMC and 0.7×CMC indicates a variation not previously reported in the literature. This difference in break-through force between different trials using conventional AFM probes with nominally the same characteristics is attributed to differences in probe geometry at the nanometer scale, a conclusion supported by the fact that the break-through forces obtained with the colloidal probe were substantially different not only in value but also in appearance (a very low positive gradient in the force vs. distance curve, which was instead high when using the regular AFM probes). However, the break-through distance values between a regular AFM probe and a colloidal probe were unchanged which indicates that the probe shape and size had no effect on the break-through distance measurements. The effects of using a probe with a different force constant on the break-through values were investigated next.

MSCT Probe "f" Trials

To study the effect of probe characteristics on break-through behavior, an f probe of the MSCT cantilever which had a stiffness ~6 times greater than the PPP-BSI probes was used. The results from force maps obtained using the PPP-BSI probe and the f probe of the MSCT

cantilever for HOPG, silica and silanated silica in 10×CMC TTAB are shown in Figure 8. Break-through distances did vary moderately beyond experimental error for some samples, but the unvarying nature was maintained between all surfaces and probes used.

Comparison of break-through force and adhesion force shows more substantial variations between surfaces and between distinct types of probes. It was found that the MSCT probe yields higher values in all cases, except for the adhesion force on silica. However, no consistent proportional relationship between the data collected with the different probes was observed. Overall, these results support our conclusion that the cantilever type does not strongly affect the measurement of the break-through distance; the average values of all three surfaces is about 3.65 nm for both probes. Conversely, both the break-through force and adhesion force are strongly probe/cantilever dependent.

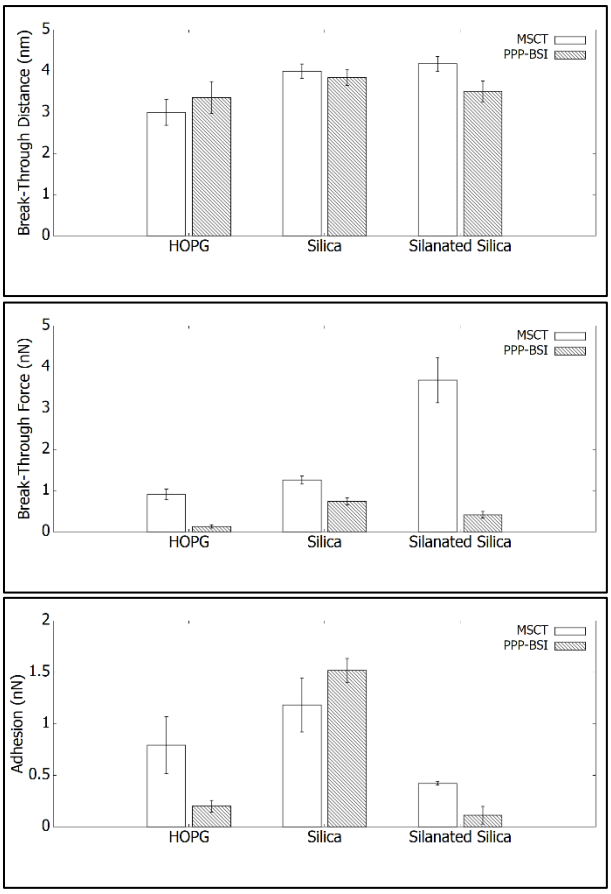

Figure 8. Break-through distance, break-through force and adhesion force using the PPP-BSI probe and the MSCT probe f at 10×CMC TTAB.

Perfusion Experiments

HOPG

During perfusion experiments the same area of adsorption can be studied as the concentration varies, reducing the opportunity for any change in the cantilever properties to occur. Our results are described below, starting from a discussion on the qualitative features of the micrographs. Discussion of the break-through force, adhesion force and break-through distance will follow.

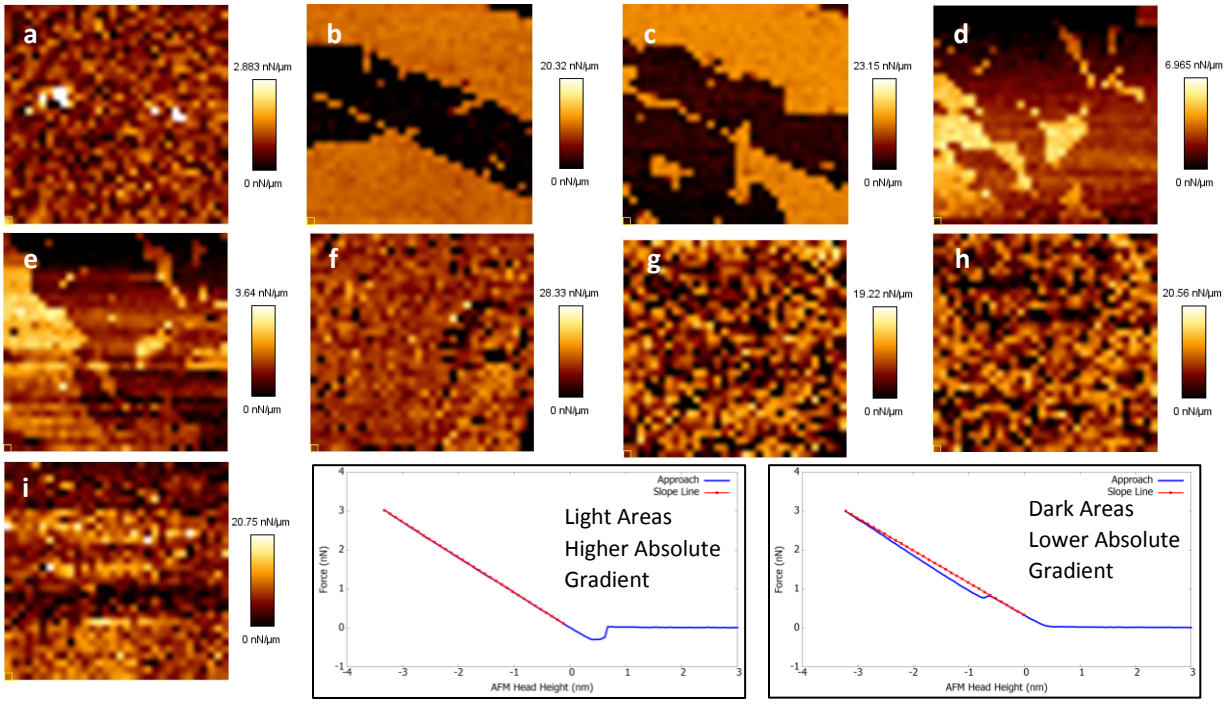

Figure 9. TTAB on HOPG-32x32 gradient maps. (a) Water (b)0.2×CMC (c) 0.2×CMC Scan 2 (d) 0.4×CMC (e) 0.6×CMC (f) 0.8×CMC (g) 2×CMC (h) 5×CMC (i) 10×CMC. All images are 5 µm × 5 µm. The force curves explain the difference between the areas of high absolute (i.e. more negative) gradient (light color on gradient map) and low absolute gradient (dark color on gradient map).

Figure 9 shows the results of perfusion experiments for pure water and TTAB at concentrations between 0.2 and 10×CMC of TTAB on HOPG. In the bottom right of Figure 9 are shown force curves, which differ from those shown previously in that there is no adjustment for deflection of the AFM cantilever and therefore the trace does not become vertical at zero on

the x-axis. By calculating gradient values in the approach curve between ~ zero on the x-axis and the maximum value before retraction was begun, it was possible to distinguish force map indices with and without break-through events during map collection. The light-colored areas in panels b–e are those in which a small or no break-through force was detected (the absolute value of the gradient is high) while the darker areas have yielded larger break-through forces (lower absolute gradient). The former is representative of little or no surfactant adsorption while the latter is representative of significant surfactant adsorption. Speckle patterns indicate insignificant variation in break-through force across the entire area of the image and are representative of little or no surfactant adsorption over the entire imaged area or a surface fully covered with surfactant (a and f-i, respectively).

In pure water (Figure 9a) the gradient image has no values that stand out appreciably from any of the others. When the surface is exposed to 0.2×CMC TTAB (Figure 9b), areas of largely differing gradient appear. The presence of areas of varying gradient suggests patchy adsorption of TTAB on HOPG. The map collected using 0.2×CMC was repeated immediately and the second dataset is shown in Figure 9c. A similar patchy structure was observed, but additional patches appear in the second scan suggesting either additional adsorption over the course of one scan (20 min.) on areas previously without break-through events or rearrangement of already adsorbed surfactant (i.e. adsorbed surfactant outside the field of view moving to inside the field of view). A more in-depth kinetic argument will be provided later in this section.

The height and lateral deflection maps (not shown) displayed no correlation with the gradient map, indicating that the break-through force heterogeneity was *not* caused by surface topography. As the bulk surfactant concentration was increased, the area of surface covered with high break-through forces also increased, as can be seen at 0.4 and 0.6×CMC (Figure 9d and

Figure 9e, respectively). When 0.8×CMC was reached, Figure 9Figure 9f, almost all the force curves displayed a break-through event which caused only small differences in gradient throughout the 5×5 µm region, resulting in the same speckle pattern noted previously, indicating the layer was complete in the observed region. Further increases in surfactant concentration, Figure 9g-i, do not change the appearance of the layer, supporting the conclusion that the layer was complete and unchanged above the CMC.

Silica

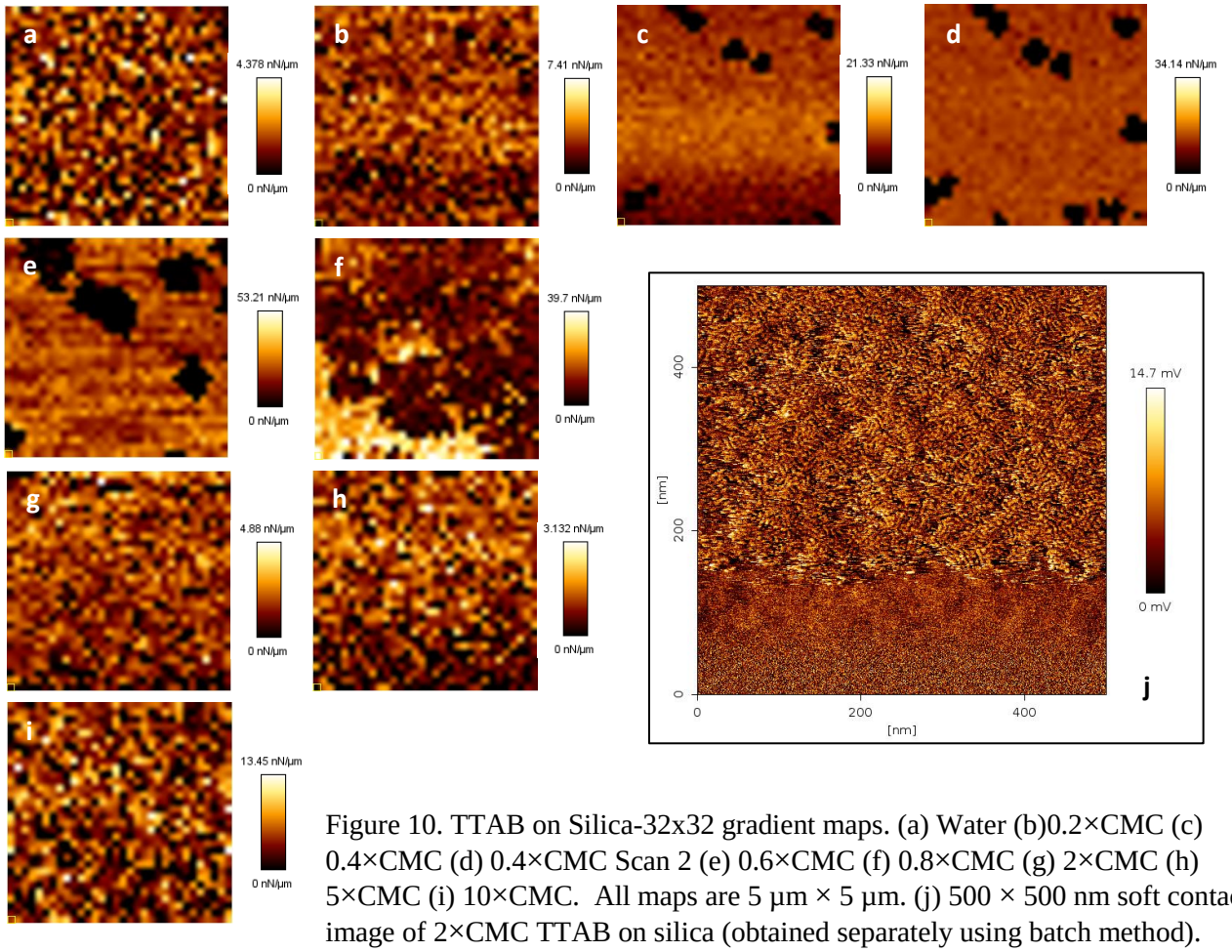

Figure 10. TTAB on Silica-32x32 gradient maps. (a) Water (b)0.2×CMC (c) 0.4×CMC (d) 0.4×CMC Scan 2 (e) 0.6×CMC (f) 0.8×CMC (g) 2×CMC (h) 5×CMC (i) 10×CMC. All maps are 5 µm × 5 µm. (j) 500 × 500 nm soft contact image of 2×CMC TTAB on silica (obtained separately using batch method).

Despite the difference in surface chemistry and wettability, the gradient maps obtained on silica (results shown in Figure 10) were like those observed on HOPG. For both pure water and

0.2×CMC TTAB, the appearance of the gradient maps (Figure 10a and Figure 10b, respectively) is the random speckle pattern, indicative of no variation in adsorption across the area of the surface. At 0.4×CMC, shown in Figure 10c and Figure 10d, small dark areas indicative of surfactant patches began to appear between subsequent scans. The fractional area covered by these patches increased between Scan 1 and Scan 2, although in this case the size of the patches was relatively constant with time. Conversely, on HOPG the size of the patches increased without an increase in their number. In fact, on HOPG the nucleation probability seems to be much less than the growth rate (compare 10c, 10d and 10e vs. 9b and 9c). Such a result is not surprising given the templating effect of the bottom layer of adsorption on HOPG. Larger patches of adsorbed surfactant appeared upon increasing the concentration to 0.6×CMC on silica, Figure 10e. Increasing the concentration to 0.8×CMC, Figure 10g, further increased the surface coverage to completeness, which remained complete for concentrations above the CMC.

None of the temporal experiments showed a lower fraction of patch-covered area with increasing time, indicating that increases in the fraction of covered area with increasing time are primarily due to increases in adsorbed amounts. In fact, our quantitative results for the fraction of covered area suggest that AFM images could be used to quantitatively measure adsorption isotherms.

Soft contact imaging of 2×CMC TTAB on silica was performed to investigate the structure of the adsorbed aggregates. The image in Figure 10j was scanned from bottom to top and the force set-point was increased until disorganized bundles of wormlike micelles became visible at around the 150 nm mark. Some difficulty occurred in acquiring images of these surfactant aggregates on silica as the probe did not remain stably above them long enough to obtain complete images, despite the several attempts we made. The reason for this difficulty is

thought to be that the force required to image the surfactant aggregates was too close to the break-through force to allow for sustained soft contact imaging.

Silanated Silica

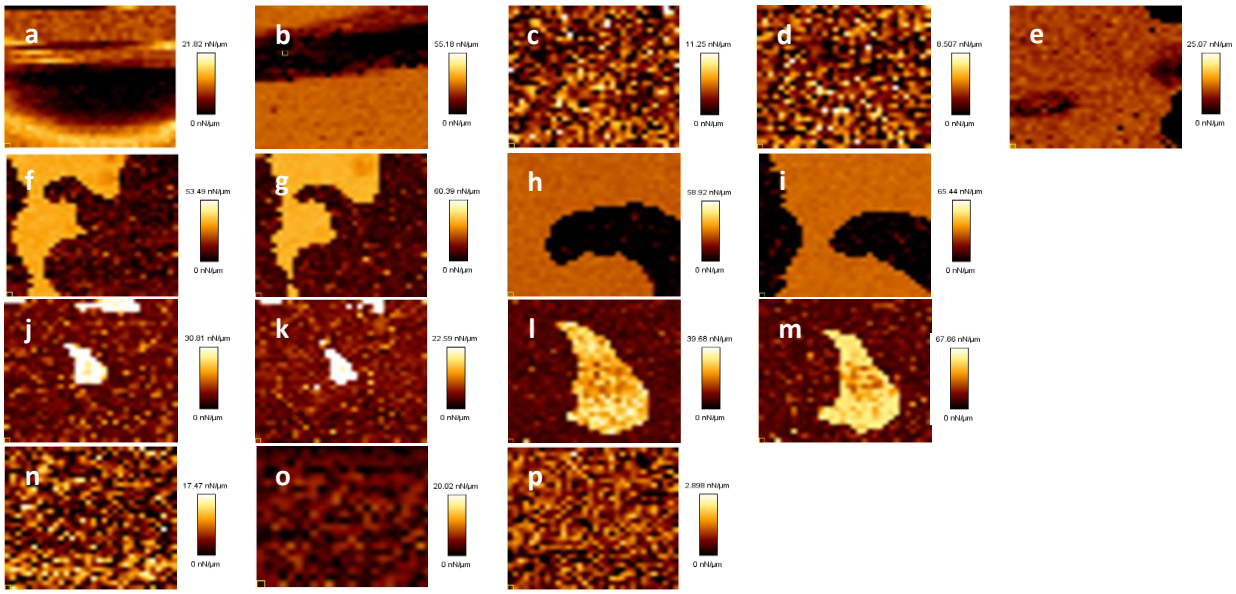

Figure 11. TTAB on Silanated Silica-32×32 force maps.

(a) Water-5 µm
(b) 0.2×CMC-5 µm
(c) 0.4×CMC-5 µm
(d) 0.6×CMC-5 µm
(e) 0.6×CMC-5 µm- Scan2
(f) 0.6×CMC-50 µm
(g) 0.6×CMC-50 µm-Scan2
(h) 0.6×CMC-15 µm
(i) 0.6×CMC-15 µm-Scan 2
(j) 0.8×CMC-50 µm
(k) 0.8×CMC-50 µm-Scan 2
(l) 0.8×CMC-15 µm
(m) 0.8×CMC-15 µm-Scan 2
(n) 2×CMC-50 µm
(o) 5×CMC-25 µm
(p) 10×CMC-50 µm

Gradient maps obtained on the silanated silica surface are shown in Figure 11. Although no break-through events were observed in the force curves obtained in water (Figure 11a), there was some variability across the map, likely caused by a bubble on the surface. Introduction of 0.2×CMC TTAB also displayed some differences in the gradient of the curves over the 5 µm area investigated, which again were likely caused by a bubble present on the surface, which moved during the collection of the force map. Surprisingly, increasing the concentration to 0.4×CMC showed a featureless surface, which appeared unchanged even when exposed to

0.6×CMC, as seen in Figure 11c and Figure 11d, respectively. However, the second 0.6×CMC map shown in Figure 11e did show two areas with break-through events in areas previously without such a feature (upper and lower right corners).

To investigate these low gradient areas further, the map size was increased to 50 μm for the two subsequent maps shown in Figure 11f and Figure 11g. Acquiring these datasets correspond to adsorption times of 70 minutes and 90 minutes at the end of each scan, respectively. The maps we collected showed non-uniform patterns, which were dynamic, as demonstrated by the slight differences in appearance between the two maps. The fractional area covered by surfactant corresponding to Figures 11f and 11g were not statistically different, indicating that the different patterns were due to slight rearrangement of the patches. The resolution of the observed area was increased by decreasing the map side length to 15 μm for Figure 11h and Figure 11i, which were also collected immediately following the map in Figure 11g and hence correspond to adsorption times of 110 and 130 minutes, respectively. Again, differences between the two maps are present, which establish the dynamic nature of the features displayed in the maps and supporting the conclusion that these were patches of adsorbed surfactant.

It was also noted from Figure 11h and Figure 11i that the distance from the left most edge of the map to the left most edge of the patch in Figure 11h is larger than the distance between the two patches in Figure 11i, by ~2 map indices. In our opinion, this result not only supports the conclusion that the changes observed between maps are not caused by the lower resolution of the larger maps, but also that the appearance of movement by the surfactant patches is not caused by AFM drift. Our reasoning is that if the apparent movement of the patches was caused by drift of the area being mapped then the distance between the two patches would not

change between maps. Furthermore, since all movement of the AFM probe near the surface is vertical, the changes with time and concentration noted here are almost certainly not caused by lateral migration induced by the AFM probe.

The concentration was increased to 0.8×CMC and two subsequent scans were acquired with a size of 50 µm, shown in Figure 11j and Figure 11k. The area of lower gradient has grown to include almost the entire map area and the size of the only remaining area without an elevated break-through force shrinks from the first to the second scan, as can also been seen in Figure 11l and Figure 11m. Further, the relative change in the fraction of covered area at 30 and 50 minutes is smaller at higher concentrations as would be expected. Further increasing the concentration to 2, 5 and 10×CMC, displayed in Figure 11n, Figure 11o and Figure 11p, led to the disappearance of the areas with lower break-through forces, again supporting the conclusion of a fully developed layer at concentrations above the CMC.

The data displayed on HOPG, silica and silanated silica in the perfusion experiments clearly demonstrate patchy adsorption (patchy adsorption was not imaged in batch experiments because the image area was much smaller in those experiments), which has been commented on in literature, usually as a part of an overall adsorption scheme involving multiple regions.[52] At low concentrations, adsorption occurs via electrostatic interactions and the fraction of surface coverage begins to rise linearly, analogous to Henry's law used with gas adsorption. Further increases in concentration yield continued adsorption to the substrate, and lateral interactions between adsorbed molecules begins to occur, promoting the aggregation of adsorbed molecules and adsorption has a dependence on the concentration. Finally, near the CMC, adsorption begins to reduce its dependency on concentration and eventually plateaus as an equilibrium between adsorption and desorption from the surface is reached.

The data obtained in this work agrees well with this phenomenological description, in that low concentrations displayed the expected patchy adsorption and those patches appear to grow with increasing concentration. Slightly below and above the CMC the maps become featureless which denotes the final region. We believe that this transition from patchy to featureless adsorption as concentration increases is the first time AFM force mapping has been used to show this behavior.

A kinetic argument can be used to determine whether changes in the maps on silica are due to adsorbing surfactant or to the migration of already adsorbed surfactant. Prior investigations studied the rate at which the similar cationic surfactant CTAB adsorbs to silica at different concentrations.[53-56] These studies agree that for concentrations above the CMC, adsorption reaches equilibrium within 30 seconds. Below the CMC the kinetics are varied, with reports of equilibrium being reached in seconds at concentrations below 0.5×CMC and the rate slowing significantly at concentrations near 0.6 mM (0.67×CMC). Both Pagac et al. and Atkin et al. observed equilibrium requiring between 11 and 3 hours at concentrations of 0.56×CMC and 0.67×CMC, respectively. As the concentration was further increased to 0.9×CMC, 90% of equilibrium was reached in only 25 minutes. In other words, the rate began decreasing at ~0.5×CMC and then increased as it was raised above 0.6×CMC.

Therefore, if we assume that TTAB behaves similarly to CTAB, we can infer that at low concentrations changes between maps are caused by surfactant migration rather than continued adsorption because each individual map was begun at least 10 minutes after surfactant was added and according to literature equilibrium is reached much more quickly. At 0.6×CMC, because equilibrium may not be reached for several hours, we cannot discriminate whether changes between maps were caused by surfactant migration or continued adsorption (although because

the differences are in patch shape and not patch size, migration is more likely). At 0.8×CMC, changes were most likely due to migration rather than adsorption since 25 minutes were required for equilibrium for CTAB at 0.9×CMC in literature. For concentrations above the CMC, equilibrium should have been reached long before the maps were begun. Unfortunately, to our knowledge, no detailed kinetic studies have been reported on HOPG with a tetramethylammonium surfactant.

Histogram Analysis of Perfusion Experiments

A typical break-through distance, break-through force and adhesion force histogram for a force map on silanated silica is shown in Figure 12. As expected from the gradient maps, two peaks are found in the break-through distance and break-through force histograms, representing the two distinct areas. Equation 2 was used to fit the two means and standard deviations for the break-through distance and break-through force, and these values are given in Table 2. Note the break-through distances in batch experiments only showed one break-through distance and force peak because only areas with surfactant that could be soft contact imaged were mapped.

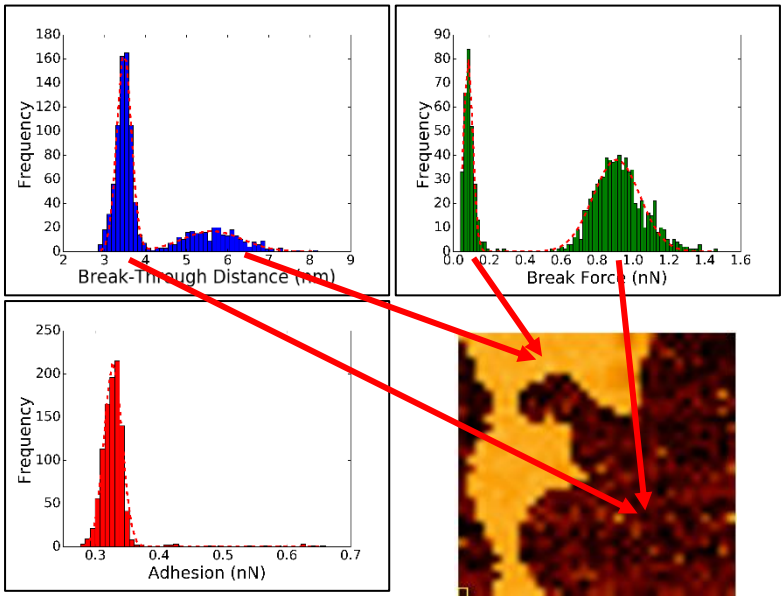

Figure 12. Break-through distance, break-through force and adhesion force histograms shown with gaussian fit results (red dotted line) for 0.6×CMC TTAB on silanated silica (Figure 11f, map shown here for reference).

The presence of two distinct peaks in the histograms and areas in the gradient maps are consistent with the dark areas (low gradient) being those with a surfactant layer capable of resisting the probe while the light areas (high gradient) have a layer which repulses the probe very little or not at all. Because the break-through force in these areas was not zero (as it was for force curves in water) the presence of an adsorbed surfactant layer adsorbed in a flat configuration was considered. However, a flat layer does not make sense with a break-through distance larger than 3.48 nm because the break-through distance should be very small (i.e. the width of a surfactant molecule). The small break-through force could result from the surfactant present on the tip generating a weak and long-ranged electrostatic double layer. Although force interactions between surfactant on a tip and a lightly-covered surface has not been shown before, a weak, long-ranged electrostatic double-layer would explain the small repulsive force between the tip and the substrate in areas with large break-through distances and makes more sense than a surface without some surfactant adsorbed.

	Break-Through Distance		Break-Through Force	
	Peak 1	Peak 2	Peak 1	Peak 2
μ	3.48	5.62	0.08	0.91
σ	0.17	0.73	0.03	0.13

Table 2. Break-through distance and break-through force means and standard deviations for two peak fitting for 0.6×CMC TTAB on silanated silica (Figure 11f)

The adhesion histogram had one main peak with mean 0.32±0.05 nN, which represents the dark (surfactant-rich) areas in the gradient map. Looking carefully at the adhesion force in Figure 12, the adhesion force in the light areas is represented by a spread of adhesion values greater than the main peak, demonstrated by the histogram bins between 0.4 nN and 0.65 nN.

This spread of values occurs due to the fewer number of points in the areas without a substantial break-through force being spread out compared to the main peak, indicating the adhesion force was more uniform in the dark areas compared to the light areas. Qualitatively, the adhesion force plots for the other two surfaces resembled those in Figure 12, as did the break-through distance and break-through force.

Using histogram analysis, the break-through distances, break-through forces and adhesion forces for the dark regions of the maps below the CMC and the entire map area above the CMC in Figures 9-11 were obtained and plotted in Figure 13. Values for the adhesion and break-through forces obtained across the three different surfaces should not be compared qualitatively because the same probes

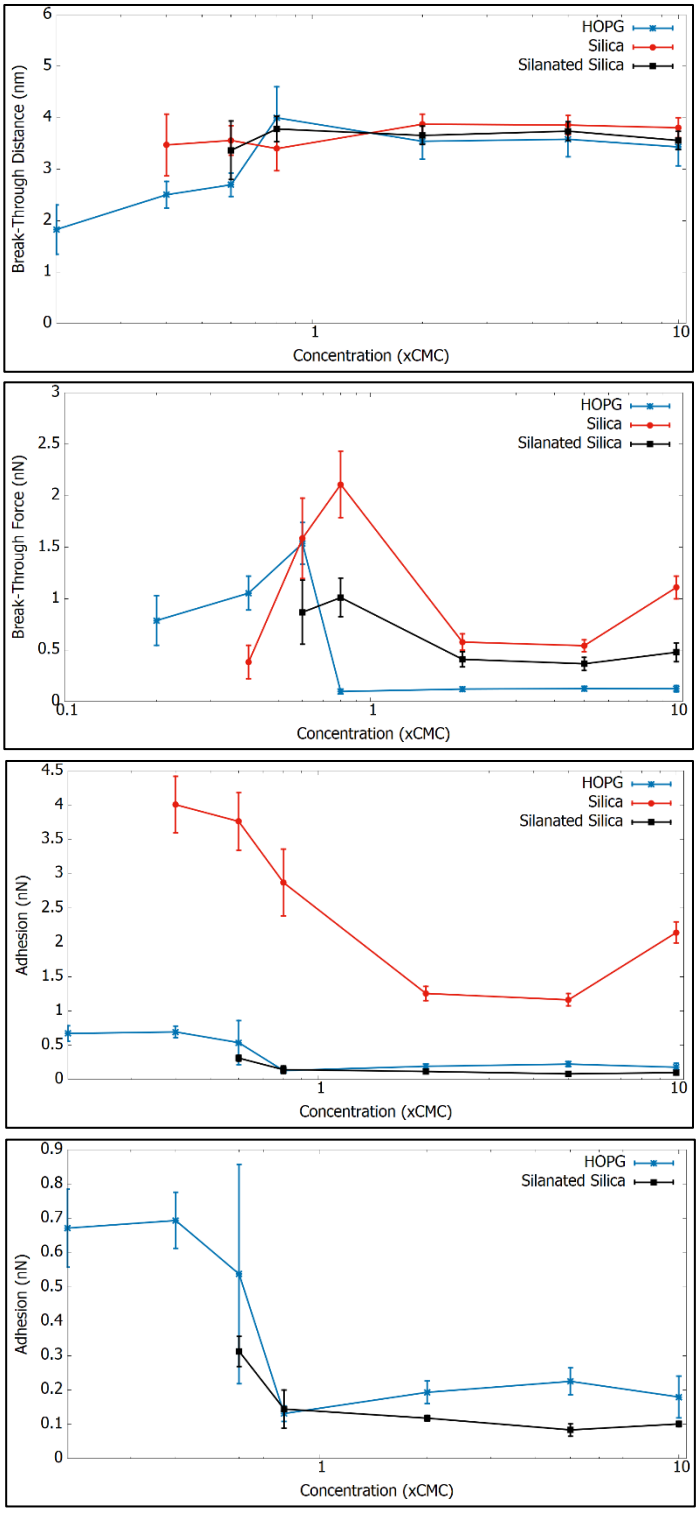

Figure 13. Break-through distance, break-through force and adhesion force from areas with surfactant on HOPG, silica and silanated silica at 0.2, 0.4, 0.6, 0.8, 2, 5 and 10×CMC of TTAB on logscale x-axis. The bottom image is a duplicate adhesion force without silica, to highlight the details of the HOPG and silanated silica traces

were not used. However, information obtained on one surface will be discussed as a function of surfactant concentration, as the tip was the same during each of these experiments.

The trend of the data on each surface shows that the break-through distances increased with increasing concentration until the CMC and then plateaued between 3.5 and 4 nm. The error associated with each value was greater below the CMC and decreased above the CMC, which we interpret as indicative of the micelle layer becoming more tightly packed above the CMC. We note that although isotherms in literature have also reported reaching the plateau region below the CMC, by far the most common result is that the start of the plateau region corresponds to the CMC. [2,57]

Break-through forces increased with increasing concentration until just below the CMC, where the values then decreased to a plateau for each surface. This is not the first time that the break-through force has been shown to increase using AFM force curves. Liu et al., Lokar et al. and Rabinovich et al. demonstrated increases in break-through force, with Liu et al. observing these increases over time at a constant concentration and the other groups observing these results using with mixed surfactant systems.[19,58,59]

In our work, a temporal explanation for the increase is less likely as the values showed no increasing trend over the course of a single map. However, the latter works suggests that adding a second component to a surfactant solution led to the changes in break-through force, which lends support to the theory of adsorbed impurities as the cause for the increase in the break-through force seen here. Such impurities would adsorb below the CMC and then above the CMC partition to micelles; hence a larger break-through force just below the CMC. QCM results in our laboratory demonstrated the same qualitative type of behavior that were also caused by

impurities at a very small level. Similar synergistic adsorption has been noted by Shi et al., who demonstrated increased adsorption and packing by using a co-solute.[60]

Above the CMC, for HOPG and silanated silica adhesion values were constant above the CMC with an increase of approximately 0.5 nN for the silica sample between 5×CMC and 10×CMC. We do not know the source of the increase.

Further discussion

Break-through distances between 3.5 and 4 nm are often found in literature using AFM and these values agree well with bilayer thicknesses found using other techniques such as neutron reflectivity and ellipsometry.[5,6,11,61] Soft contact imaging has revealed spherical or cylindrical micelles on silica both here and in other publications and as previously mentioned it is accepted that monolayer thickness structures (monolayers and hemi-cylinders/spheres) form on hydrophobic surfaces and bilayer thickness structures (bilayers and full cylinders/spheres) form on hydrophilic surfaces. [11,12,24,29] Why then do the break-through distances differ only slightly between the hydrophilic and hydrophobic surfaces? Compression via the AFM probe was considered as to why the break-through distance values are so similar. However, using compression to explain the equivalence seems unlikely because other techniques involving no physical contact have been used to show a difference in the thickness of adsorbed surfactant when AFM could not, even when using similar surfaces.[5,6,40]

While our results alone are not irrefutable proof, the fact that the break-through distance of a surfactant layer on an AFM tip was found to be like those found on flat surfaces using colloidal and regular AFM probes increases the doubt that the break-through distance is a reliable measure of surface adsorbed surfactant layer thickness. Rephrasing our question, why is the break-through distance the same for two hydrophobic surfaces, two hydrophilic surfaces or one hydrophobic and one hydrophilic surface? Figure 14 addresses these some of these points.

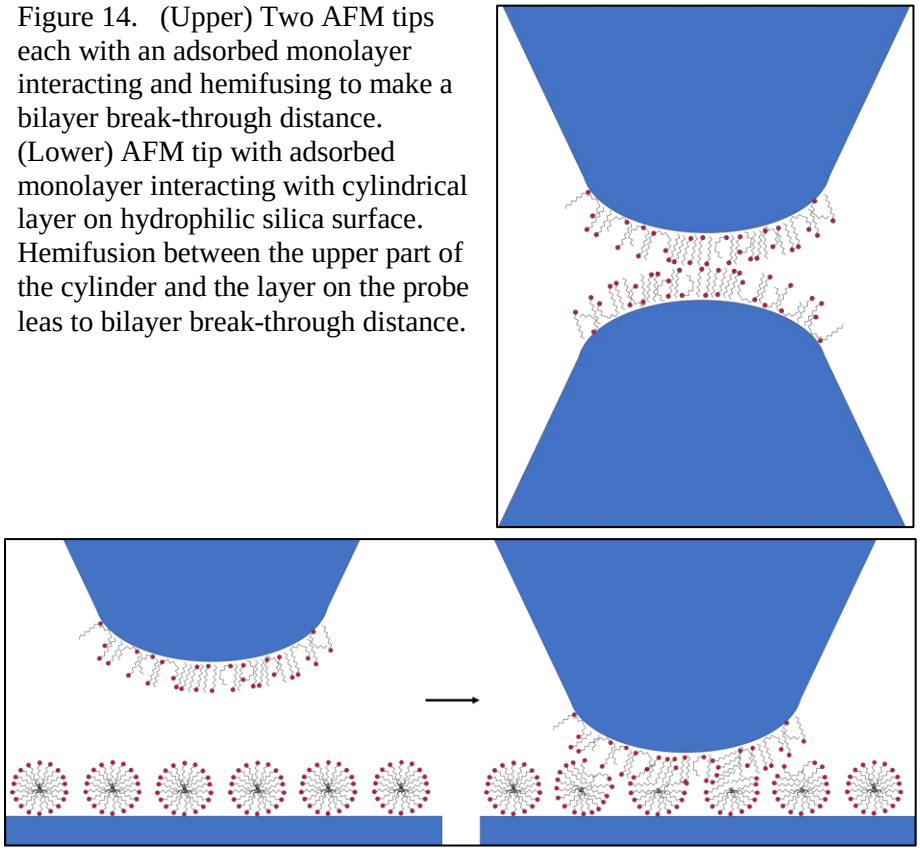

Figure 14. (Upper) Two AFM tips each with an adsorbed monolayer interacting and hemifusing to make a bilayer break-through distance. (Lower) AFM tip with adsorbed monolayer interacting with cylindrical layer on hydrophilic silica surface. Hemifusion between the upper part of the cylinder and the layer on the probe leas to bilayer break-through distance.

First, we take the case of two monolayers, such as would be found between two AFM tips or between an AFM tip and a hydrophobic surface. In the case of an AFM tip, little is known about the orientation/packing of this layer, but we hypothesize that due to geometry and surface conditions the layer is not well packed and there are possibly molecules adsorbed in multiple orientations (although a majority will be tail down). As the two surfaces come into contact, there will be repulsion from molecules whose headgroups are facing the layer on the other surface and

once the layers are in contact the tip breaks through both layers simultaneously to yield a bilayer thickness break-through distance.

Second, we consider the cases which have a bilayer present. Figure 4 and the associated discussion describes what happens when two bilayers are present as determined via SFA studies; the upper layers from each bilayer diffuse to the surrounding solution or reorient so that the tails of the surface adsorbed layers may interact and again a bilayer break-through distance results.

Next, the situation visualized in Figure 14, wherein a hydrophilic silica surface, which would have a bilayer, is approached by an AFM tip with an adsorbed monolayer. Reorientation of the bilayer (or perhaps desorption of surfactant from the tip given the likely disordered nature of the monolayer on the tip) results in a single bilayer between the probe and the surface prior to break-through. The same argument can be made in the case for a colloidal probe (adsorbed bilayer) and HOPG (hydrophobic flat surface); however, complete desorption of surfactant from HOPG seems unlikely as literature has shown that the monolayer on HOPG is irreversibly adsorbed due to the strong interaction between the tails of the surfactant and the graphene rings of HOPG.[62]

We were surprised in the case of one bilayer and one monolayer that the break-through distance matched that of a single bilayer because of the difficulties suggested by Figure 14. If correct, then this hypothesis would explain why bilayers measured using contact free methods agree so closely with surfactant layers measured using AFM. It would be interesting to use a chemically-modified tip such as Pera et al. used to study lipid bilayers using force curves.[34] In their work, if the tip or surface were independently modified (so that only one bilayer was present) there was only one break-through event. However, if both the tip and the surface were modified then two break-through events were observed. Their chemical modification was

thought to strengthen the adsorption of the lipid and produce bilayers on their AFM tips, which, along with the typical differences between adsorbed layers of lipid and surfactant, is most likely why we saw no double break-through events in our work.

The ability to distinguish adsorbed patches using AFM gradient mapping has several implications for future research. For example, surface chemistry could be varied in a regular manner and adsorption as a function of surface chemistry could be measured. Once this is accomplished, the dimensions of the surface variation could be altered. Such a study would allow one to determine the length scale over which surface chemistry variation is important. This type of study would have relevance for corrosion since non-adsorption of a corrosion inhibitor at a very local area could be distinguished. As another example, we plan to publish studies using the techniques in this paper to examine how adsorption changes on the flat tops of pillars where the area of the top varies. Real surfaces are very rarely molecularly smooth or chemically homogeneous; the techniques described in this paper are ideal for exploring how variations in topology or surface chemistry affect adsorption, providing experimental validation for recent simulation results.[63,64]

Conclusions

Force mapping between two AFM tips verified a surfactant layer on an AFM tip using a set-up which did not use a flat surface. Results from force mapping with a colloidal probe and a probe with a different force constant demonstrated that the probe geometry and force constant influenced the break-through force and adhesion force but not break-through distance. Very slight differences, such as tip cleaning between trials, can alter force data values.

Gradient mapping was performed on flat HOPG, silica and silanated silica surfaces and the data showed patches of adsorbed surfactant below the CMC. While the results are consistent

with others available in the literature, this is the first time AFM force curves with mapping are used to observe adsorbed surfactants at different times, which in turn gives information about the spatial nature of adsorption. Evidence of changing adsorption density with time is reported. Even at long times, where adsorption density did not change, spatial distribution of adsorbed surfactant patches continued to shift shape/position. With increasing concentration below the CMC, the break-through distance and break-through force increased while the adhesion force decreased.

Break-through force was maximum at the CMC, which was attributed to the well-known impurity effect found in some surface tension plots although further studies would be needed to confirm this conclusion. Very surprisingly, above the CMC the break-through distance did not depend on whether the surface was hydrophilic or hydrophobic. A qualitative phenomenological theory was developed analogous to a theory previously developed to explain surface force apparatus results from two hydrophilic surfaces. Based on our interpretation, break-through events can be interpreted as a measure of the coverage or stability of the adsorbed layer; however, the break-through distance does not necessarily represent the thickness of an adsorbed bilayer due to hemifusion/convolution by an adsorbed layer on the AFM probe.

Acknowledgements

Primary financial support was provided by the National Science Foundation under Grant No. CMMI–1068705 as well the American Australian Association for funding JJ Hamon to spend a year in Australia through the Sir Keith Murdoch fellowship. We would also like to thank support from the U.K. Engineering and Physical Sciences Research Council under grant number EP/N007123/1 to AS, an ARC Future Fellowship (FT160100191) to RFT and the industrial sponsors of the Institute for Applied Surfactant Research (IASR) at the University of Oklahoma for BPG.

References

(1) Wu, S. Q.; Shi, L.; Garfield, L. B.; Tabor, R. F.; Striolo, A.; Grady, B. P. Influence of Surface Roughness on Cetyltrimethylammonium Bromide Adsorption from Aqueous Solution. *Langmuir* **2011**, *27*, 6091-6098.

(2) Gutig, C.; Grady, B. P.; Striolo, A. Experimental studies on the adsorption of two surfactants on solid-aqueous interfaces: Adsorption isotherms and kinetics. *Langmuir* **2008**, *24*, 13814-13814.

(3) Macakova, L.; Blomberg, E.; Claesson, P. M. Effect of adsorbed layer surface roughness on the QCM-D response: Focus on trapped water. *Langmuir* **2007**, *23*, 12436-12444.

(4) Bordes, R.; Hook, F. Separation of Bulk Effects and Bound Mass during Adsorption of Surfactants Probed by Quartz Crystal Microbalance with Dissipation: Insight into Data Interpretation. *Anal. Chem.* **2010**, *82*, 9116-9121.

(5) Fragneto, G.; Thomas, R. K.; Rennie, A. R.; Penfold, J. Neutron reflection from hexadecyltrimethylammonium bromide adsorbed on smooth and rough silicon surfaces. *Langmuir* **1996**, *12*, 6036-6043.

(6) Tiberg, F. Physical characterization of non-ionic surfactant layers adsorbed at hydrophilic and hydrophobic solid surfaces by time-resolved ellipsometry. *J. Chem. Soc., Faraday Trans.* **1996**, *92*, 531-538.

(7) Berry, J. D.; Neeson, M. J.; Dagastine, R. R.; Chan, D. Y. C.; Tabor, R. F. Measurement of surface and interfacial tension using pendant drop tensiometry. *J. Colloid Interface Sci.* **2015**, *454*, 226-237.
(8) Yoon, R.-H.; Yordan, J. L. Zeta-potential measurements on microbubbles generated using various surfactants. *J. Colloid Interface Sci.* **1986**, *113*, 430-438.
(9) Sun, Z.; Nicolosi, V.; Rickard, D.; Bergin, S. D.; Aherne, D.; Coleman, J. N. Quantitative Evaluation of Surfactant-stabilized Single-walled Carbon Nanotubes: Dispersion Quality and Its Correlation with Zeta Potential. *J. Phys. Chem. C* **2008**, *112*, 10692-10699.
(10) Lin, D. C.; Dimitriadis, E. K.; Horkay, F. Robust Strategies for Automated AFM Force Curve Analysis—I. Non-adhesive Indentation of Soft, Inhomogeneous Materials. *J. Biomech. Eng.* **2006**, *129*, 430-440.
(11) Velegol, S. B.; Fleming, B. D.; Biggs, S.; Wanless, E. J.; Tilton, R. D. Counterion Effects on Hexadecyltrimethylammonium Surfactant Adsorption and Self-Assembly on Silica. *Langmuir* **2000**, *16*, 2548-2556.
(12) Saville, D. A.; Chun, J.; Li, J. L.; Schniepp, H. C.; Car, R.; Aksay, I. A. Orientational Order of Molecular Assemblies on Inorganic Crystals. *Phys. Rev. Lett.* **2006**, *96*, 018301.
(13) Wanless, E. J.; Ducker, W. A. Weak Influence of Divalent Ions on Anionic Surfactant Surface-Aggregation. *Langmuir* **1997**, *13*, 1463-1474.
(14) Wanless, E. J.; Davey, T. W.; Ducker, W. A. Surface Aggregate Phase Transition. *Langmuir* **1997**, *13*, 4223-4228.
(15) Manne, S.; Cleveland, J. P.; Gaub, H. E.; Stucky, G. D.; Hansma, P. K. Direct Visualization of Surfactant Hemimicelles by Force Microscopy of the Electrical Double Layer. *Langmuir* **1994**, *10*, 4409-4413.
(16) Manne, S.; Gaub, H. E. Molecular-Organization of Surfactants at Solid-Liquid Interfaces. *Science* **1995**, *270*, 1480-1482.
(17) Blom, A.; Warr, G. G.; Wanless, E. J. Morphology Transitions in Nonionic Surfactant Adsorbed Layers near Their Cloud Points. *Langmuir* **2005**, *21*, 11850-11855.
(18) Schniepp, H. C.; Saville, D. A.; Aksay, I. A. Tip-Induced Orientational Order of Surfactant Micelles on Gold. *Langmuir* **2008**, *24*, 626-631.

(19) Liu, J.-F.; Ducker, W. A. Surface-Induced Phase Behavior of Alkyltrimethylammonium Bromide Surfactants Adsorbed to Mica, Silica, and Graphite. *J. Phys. Chem. B* **1999**, *103*, 8558-8567.
(20) Liu, J.-F.; Min, G.; Ducker, W. A. AFM Study of Adsorption of Cationic Surfactants and Cationic Polyelectrolytes at the Silica−Water Interface. *Langmuir* **2001**, *17*, 4895-4903.
(21) Künneke, S.; Krüger, D.; Janshoff, A. Scrutiny of the Failure of Lipid Membranes as a Function of Headgroups, Chain Length, and Lamellarity Measured by Scanning Force Microscopy. *Biophys. J.* **2004**, *86*, 1545-1553.
(22) Lima, L. M. C.; Giannotti, M. I.; Redondo-Morata, L.; Vale, M. L. C.; Marques, E. F.; Sanz, F. Morphological and Nanomechanical Behavior of Supported Lipid Bilayers on Addition of Cationic Surfactants. *Langmuir* **2013**, *29*, 9352-9361.
(23) Senden, T. J.; Drummond, C. J.; Kekicheff, P. Atomic Force Microscopy: Imaging with Electrical Double Layer Interactions. *Langmuir* **1994**, *10*, 358-362.
(24) Li, J.; Zhang, C.; Cheng, P.; Chen, X.; Wang, W.; Luo, J. AFM Studies on Liquid Superlubricity between Silica Surfaces Achieved with Surfactant Micelles. *Langmuir* **2016**, *32*, 5593-5599.
(25) Schniepp, H. C.; Shum, H. C.; Saville, D. A.; Aksay, I. A. Surfactant Aggregates at Rough Solid−Liquid Interfaces. *J. Phys. Chem. B* **2007**, *111*, 8708-8712.
(26) Butt, H.-J.; Franz, V. Rupture of molecular thin films observed in atomic force microscopy. I. Theory. *Phys. Rev. E.* **2002**, *66*, 031601.
(27) Micklavzina, B. L.; Zhang, S.; He, H.; Longo, M. L. Nanomechanical Characterization of Micellar Surfactant Films via Atomic Force Microscopy at a Graphite Surface. *Langmuir* **2017**, *33*, 2122-2132.
(28) Li, J. K.; Sullan, R. M. A.; Zou, S. Atomic Force Microscopy Force Mapping in the Study of Supported Lipid Bilayers. *Langmuir* **2011**, *27*, 1308-1313.
(29) Sakai, K.; Matsuhashi, K.; Honya, A.; Oguchi, T.; Sakai, H.; Abe, M. Adsorption Characteristics of Monomeric/Gemini Surfactant Mixtures at the Silica/Aqueous Solution Interface. *Langmuir* **2010**, *26*, 17119-17125.
(30) Subramanian, V.; Ducker, W. A. Counterion Effects on Adsorbed Micellar Shape: Experimental Study of the Role of Polarizability and Charge. *Langmuir* **2000**, *16*, 4447-4454.

(31) Kobayashi, N.; Saitoh, H.; Kawamura, R.; Yoshikawa, H. Y.; Nakabayashi, S. Structural change of nonionic surfactant self-assembling at electrochemically controlled HOPG/electrolyte interface. *J. Electroanal. Chem.* **2017**, *799*, 444-450.
(32) Franz, V.; Loi, S.; Müller, H.; Bamberg, E.; Butt, H.-J. Tip penetration through lipid bilayers in atomic force microscopy. *Colloids and Surfaces B: Biointerfaces* **2002**, *23*, 191-200.
(33) Loi, S.; Sun, G.; Franz, V.; Butt, H. J. Rupture of molecular thin films observed in atomic force microscopy. II. Experiment. *Phys. Rev. E.* **2002**, *66*, 031602.
(34) Pera, I.; Stark, R.; Kappl, M.; Butt, H.-J.; Benfenati, F. Using the Atomic Force Microscope to Study the Interaction between Two Solid Supported Lipid Bilayers and the Influence of Synapsin I. *Biophys. J.* **2004**, *87*, 2446-2455.
(35) Zou, Y.; Jayasuriya, S.; Manke, C. W.; Mao, G. Influence of Nanoscale Surface Roughness on Colloidal Force Measurements. *Langmuir* **2015**, *31*, 10341-10350.
(36) Garcia-Manyes, S.; Redondo-Morata, L.; Oncins, G.; Sanz, F. Nanomechanics of Lipid Bilayers: Heads or Tails? *J. Am. Chem. Soc.* **2010**, *132*, 12874-12886.
(37) Stiernstedt, J.; Fröberg, J. C.; Tiberg, F.; Rutland, M. W. Forces between Silica Surfaces with Adsorbed Cationic Surfactants: Influence of Salt and Added Nonionic Surfactants. *Langmuir* **2005**, *21*, 1875-1883.
(38) Vautier-Giongo, C.; Bales, B. L. Estimate of the Ionization Degree of Ionic Micelles Based on Krafft Temperature Measurements. *J. Phys. Chem. B* **2003**, *107*, 5398-5403.
(39) Kozbial, A.; Trouba, C.; Liu, H.; Li, L. Characterization of the Intrinsic Water Wettability of Graphite Using Contact Angle Measurements: Effect of Defects on Static and Dynamic Contact Angles. *Langmuir* **2017**, *33*, 959-967.
(40) Stålgren, J. J.; Eriksson, J.; Boschkova, K. A Comparative Study of Surfactant Adsorption on Model Surfaces Using the Quartz Crystal Microbalance and the Ellipsometer. *J. Colloid Interface Sci.* **2002**, *253*, 190-195.
(41) Ducker, W. A.; Grant, L. M. Effect of Substrate Hydrophobicity on Surfactant Surface−Aggregate Geometry. *J. Phys. Chem.* **1996**, *100*, 11507-11511.
(42) Butt, H.-J.; Cappella, B.; Kappl, M. Force measurements with the atomic force microscope: Technique, interpretation and applications. *Surf. Sci. Rep.* **2005**, *59*, 1-152.
(43)Biggs, S.; Mulvaney, P. In *Surfactant Adsorption and Surface Solubilization*; American Chemical Society, 1996, pp 255-266.

(44) Donaldson, S. H.; Lee, C. T.; Chmelka, B. F.; Israelachvili, J. N. General hydrophobic interaction potential for surfactant/lipid bilayers from direct force measurements between light-modulated bilayers. *Proc. Natl. Acad. Sci.* **2011**, *108*, 15699-15704.
(45) Podgornik, R.; Parsegian, V. A. Forces between CTAB-Covered Glass Surfaces Interpreted as an Interaction-Driven Surface Instability. *J. Phys. Chem.* **1995**, *99*, 9491-9496.
(46) Helm, C. A.; Israelachvili, J. N.; McGuiggan, P. M. Molecular mechanisms and forces involved in the adhesion and fusion of amphiphilic bilayers. *Science* **1989**, *246*, 919-922.
(47) Subramanian, V.; Ducker, W. Proximal Adsorption of Cationic Surfactant on Silica at Equilibrium. *J. Phys. Chem. B* **2001**, *105*, 1389-1402.
(48) Chun, J.; Li, J.-L.; Car, R.; Aksay, I. A.; Saville, D. A. Anisotropic Adsorption of Molecular Assemblies on Crystalline Surfaces. *J. Phys. Chem. B* **2006**, *110*, 16624-16632.
(49) Wanless, E. J.; Ducker, W. A. Organization of Sodium Dodecyl Sulfate at the Graphite−Solution Interface. *J. Phys. Chem.* **1996**, *100*, 3207-3214.
(50) Warr, G. G. Surfactant adsorbed layer structure at solid/solution interfaces: impact and implications of AFM imaging studies. *Current Opinion in Colloid & Interface Science* **2000**, *5*, 88-94.
(51) Tiberg, F.; Brinck, J.; Grant, L. Adsorption and surface-induced self-assembly of surfactants at the solid–aqueous interface. *Current Opinion in Colloid & Interface Science* **1999**, *4*, 411-419.
(52) Paria, S.; Khilar, K. C. A review on experimental studies of surfactant adsorption at the hydrophilic solid-water interface. *Adv. Colloid Interface Sci.* **2004**, *110*, 75-95.
(53) Atkin, R.; Craig, V. S. J.; Biggs, S. Adsorption Kinetics and Structural Arrangements of Cationic Surfactants on Silica Surfaces. *Langmuir* **2000**, *16*, 9374-9380.
(54) Pagac, E. S.; Prieve, D. C.; Tilton, R. D. Kinetics and Mechanism of Cationic Surfactant Adsorption and Coadsorption with Cationic Polyelectrolytes at the Silica−Water Interface. *Langmuir* **1998**, *14*, 2333-2342.
(55) Woods, D. A.; Petkov, J.; Bain, C. D. Surfactant Adsorption Kinetics by Total Internal Reflection Raman Spectroscopy. 1. Pure Surfactants on Silica. *J. Phys. Chem. B* **2011**, *115*, 7341-7352.
(56) Howard, S. C.; Craig, V. S. J. Adsorption of the Cationic Surfactant Cetyltrimethylammonium Bromide to Silica in the Presence of Sodium Salicylate: Surface Excess and Kinetics. *Langmuir* **2009**, *25*, 13015-13024.

(57) Lajtar, L.; Narkiewicz-Michalek, J.; Rudzinski, W.; Partyka, S. A New Theoretical Approach to Adsorption of Ionic Surfactants at Water/Oxide Interfaces: Studies of the Mechanism of Cationic Surfactant Adsorption. *Langmuir* **1994**, *10*, 3754-3764.
(58) Rabinovich, Y. I.; Pandey, S.; Shah, D. O.; Moudgil, B. M. Effect of the Chain-Length Compatibility of Surfactants and Mechanical Properties of Mixed Micelles on Surfaces. *Langmuir* **2006**, *22*, 6858-6862.
(59) Lokar, W. J.; Ducker, W. A. Forces between Glass Surfaces in Mixed Cationic−Zwitterionic Surfactant Systems. *Langmuir* **2004**, *20*, 4553-4558.
(60) Shi, L.; Ghezzi, M.; Caminati, G.; Lo Nostro, P.; Grady, B. P.; Striolo, A. Adsorption Isotherms of Aqueous C12E6 and Cetyltrimethylammonium Bromide Surfactants on Solid Surfaces in the Presence of Low Molecular Weight Coadsorbents. *Langmuir* **2009**, *25*, 5536-5544.
(61) Rennie, A. R.; Lee, E. M.; Simister, E. A.; Thomas, R. K. Structure of a cationic surfactant layer at the silica-water interface. *Langmuir* **1990**, *6*, 1031-1034.
(62) Király, Z.; Findenegg, G. H. Pulsed-Flow Microcalorimetric Study of the Template-Monolayer Region of Nonionic Surfactants Adsorbed at the Graphite/Water Interface. *Langmuir* **2005**, *21*, 5047-5054.
(63) Suttipong, M.; Grady, B. P.; Striolo, A. Surfactant Aggregates Templated by Lateral Confinement. *J. Phys. Chem. B* **2015**, *119*, 5467-5474.
(64) Suttipong, M.; Grady, B. P.; Striolo, A. Surfactants adsorption on crossing stripes and steps. *Soft Matter* **2017**, *13*, 862-874.

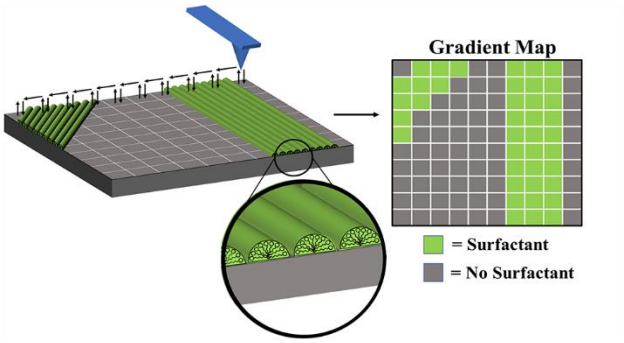
Gradient Map
= Surfactant
= No Surfactant